NUMERICAL RESULTS FOR HEAT TRANSFER AND MHD SLIP FLOW OF POWER-LAW NANOFLUID OVER AN INFINITE ROTATING DISK

by

AMNA SADIQ

A Dissertation submitted for the degree of

Master of Science in Mathematics.

Supervised by

DR. ASIM AZIZ

DEPARTMENT OF MATHEMATICS
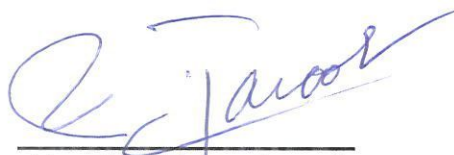
SCHOOL OF NATURAL SCIENCES (SNS)

NATIONAL UNIVERSITY OF SCIENCES AND TECHNOLOGY (NUST)

ISLAMABAD, PAKISTAN

FORM TH-4

National University of Sciences & Technology

MS THESIS WORK

We hereby recommend that the dissertation prepared under our supervision by: MS. AMNA SADIQ, Regn No. 00000106841 Titled Numerical Results for Heat Transfer and MHD Slip Flow of Power Law Nanofluid Over an Infinite Rotating Disk be accepted in partial fulfillment of the requirements for the award of **MS** degree.

Examination Committee Members

1. Name: DR. MUHAMMAD ASIF FAROOQ   Signature: _____

2. Name: DR. TAYYAB HUSSAIN SHAH   Signature: _____

External Examiner: PROF. SOHAIL NADEEM   Signature: _____

Supervisor's Name DR. ASIM AZIZ   Signature: _____

_____
Head of Department

22/11/2018
_____
Date

COUNTERSINGED

Date: 22/11/2018

_____
Dean/Principal

THESIS ACCEPTANCE CERTIFICATE

Certified that final copy of MS thesis written by **Ms. Amna Sadiq** (Registration No. **00000106841**), of **School of Natural Sciences** has been vetted by undersigned, found complete in all respects as per NUST statutes/regulations, is free of plagiarism, errors, and mistakes and is accepted as partial fulfillment for award of MS/M.Phil degree. It is further certified that necessary amendments as pointed out by GEC members and external examiner of the scholar have also been incorporated in the said thesis.

Signature: _____

Name of Supervisor: Dr. Asim Aziz_____

Date: _____22/11/2018_____

Signature (HoD): _____

Date: _____22/11/2018_____

Signature (Dean/Principal): _____

Date: _____22/11/2018_____

Dedicated to

my mother for her endless love, support and encouragement

and my father (late) for his love and prayers.

ACKNOWLEDGMENTS

In the name of Almighty Allah, the most merciful and the benevolent. I am thankful and greatly obliged to Him for showering me with His countless blessings and continuous assistance in every phase of life.

Firstly, I would like to express my deepest gratitude to my supervisor **Dr. Asim Aziz**, for his generous support, guidance and encouragement throughout research phase.

Secondly, I also want to pay my regards to my GEC members, Dr. Tayyab Hussain Shah (C EME) and Dr. Muhammad Asif Farooq (SNS) for providing their precious time and guidance.

I am also thankful to the Principle SNS Dr. Habib Nasir and HOD Mathematics Dr. Rashid Farooq and all the faculty members of Mathematics department, for helping, teaching and guiding me during MS studies.

I would like to express my deepest gratitude to my parents and siblings for their endless prayers, love, continuous encouragement and moral support.

Amna Sadiq

ABSTRACT

The analysis of nanofluid flow under the influence of rotation effects has been given great significance in recent years because it has various applications in industries like in power generating units, rotating machinery, solar collectors, nuclear reactor system etc. This dissertation investigates the problem which deals with MHD slip flow and heat transfer of Cu-water and Al_2O3-water nanofluids. The fluid occupies the space over an infinite rotating disk. Here, thermal conductivity of the nanofluid is considered as a function of velocity gradients only. The non-linearity of the governing equations are removed by first applying similarity transformation which are invoked to remodel the governing system then solving it computationally by using *bvp4c* solver in MATLAB. The graphical results are presented against various different parameters and are used to analyze the effect of POWER-LAW index, solid volume fraction, slip and MHD parameters on fluid's motion and temperature profiles. The tabular results are also presented to depict the effect of variations in heat transfer rate and motion at the boundary. It has been concluded that addition of nanoparticles and presence of strong magnetic field increases the thermal behavior of fluid. Moreover, the increase in magnitude of magnetic field causes decrease in the velocity of fluid.

Contents

Chapter 1

INTRODUCTION

Heat transfer caused by to fluid flow is a trust area of research in the field of fluid mechanics. Therefore processes including heat transfer has been given great attention by the researchers in recent years. Heat transfer through fluid flow has applications in industries for example, heat exchangers, cooling systems, refrigeration, chemical plants, solar collectors, nuclear reactor system, optical modulators, optical switches, biomedicine. Analysis of any model which includes heat transfer is influenced by many factors like geometry of the flow, viscosity of the fluid, flow medium, boundary conditions, thermal conductivity etc.

Maxwell [1] first suggested that we can increase the thermal conductivity of fluid by including solid particles in the fluid which is the main idea behind the theory of nanofluids. Choi [2] first introduced the term nanofluid by including suspension of solid nanometer sized particles (Cu, Ag etc) in heat transfer base fluids (oil, water, ethynol etc). Nanofluids enhanced the heat transfer characteristics of ordinary fluids because the inclusion of nanoparticles helps in conducting heat transfer at molecular level. Eastman et al. [3] extended the work on nanofluids and noticed enhancement in thermal conductivity and heat transfer rate of Cu-nanofluids when the volume fraction of nanoparticles was kept small. The increase in thermal properties of

1

nanofluids was experimentally proved by both Wang et al. [4] and Keblinski et al. [5]. Buongiorno [6] presented a comprehensive study on convective transport in nanofluids. The detailed review of literature on nanofluids models can be found in the studies of Keblinski et al. [7] and Wang and Mujumdar [8]. Noghrehabadi et al. [9] studied the effects of variation in nanofluid's chemical structure over a vertical plate. Results presented in [10–12] and the aforementioned studies confirm that the nanofluids has higher thermal conductivity than ordinary fluids. Turkyilmazoglu [13] considered five types of water-based nanofluids. He found that the transfer of heat from boundary is enhanced by the addition of nanoparticles. Makinde and Aziz [14] conducted a study on boundary layer flow of nanofluid. Their model include flow over a stretching flat surface. Hayat et al. [15] discussed nanofluid flow between two rotating disks. Their model include effects of MHD and boundary slip. Authors are recommended to study [16–20] for further insight into the effects of variable nanofluid properties.

Application of nanofluids in industrial sector includes, for example in many nuclear processes they act as coolant, industrial cooling applications, oil extraction process, computer processors, thermal solar collectors, biological solutions, micro-electromechanical systems, hybrid-powered engine, paints, glues and automobiles. Cooling rate in electronic devices can be improved using nanofluids. Magnetic nanofluid like ferrofluid also have prominent role in cancer treatment, drug delivery etc. Woong and Leon [21] and Saidur et al. [22] in their review work highlighted many applications of nanofluids in the areas of biomedical, automotive, electronics etc.

In all above-mentioned studies Newtonian fluid model is considered to study the flow of nanofluids through different geometries. Generally nanofluids do not behave like Newtonian fluids. Therefore non-Newtonian fluid models are more appropriate to study the nanfluids models. Many authors presented non-Newtonian fluid models

and their details are easily available in literature. It is beyond the scope of this study to discuss all the non-Newtonian fluid models. The POWER-LAW rheology is the simplest non-Newtonian fluid model in which consistency and flow behavior indexes are enough for classification of different types of fluids.

Rotating flows exist in various industrial and engineering processes such as turbine system, electric power generating system, extraction of crude oil from petroleum products, filtration processes, synthetic fibers, food processing industries, jet motors etc. They also have many geophysical applications like the dynamics of tornadoes and cyclones, geothermal extraction etc. Cochran [23] first studied the rotating disk flow using Von Karman transformations. Stewartson [24] examined rotating flow between two disks. Ming et al. [25] investigated the heat transfer and flow of power–law fluid induced due to rotation of disk and obtained suitable similarity solutions. Their model included the assumption proposed by Pop et al. [26, 27]. That is the thermal conductivity depends on the velocity derivatives. They discussed the results for various physical parameters like POWER-LAW index and solid volume fraction which directly effects the flow, heat and mass transfer. It was also found that thermal conduction is stronger for higher Prandtl number. Kumari et al. [28] investigated the non-Newtonian flow of a steady and rotating POWER-LAW fluid over a stretching surface. Khan et al. [29] did the numerical study for rotating flow of nanofluids driven by convectively heated surface. In a recent study Ming et al. [30] analyzed the POWER-LAW fluid flow and heat transfer induced by a rotating disk with generalized diffusion. Saleem et al. [31] worked on MHD POWER-LAW fluid model including the influence of Hall effects over a rotating disk to examine the effect of variations of various parameters on Cu-water.

Von Karman [32] initiated the first study on fluid flow of over a rotating surface. Several authors extended the benchmark problem of Von Karman by including the non-Newtonian fluid over a spinning disk. The flow is now no longer governed by

Navier-Stokes equations but by the well known Cauchy equations. Due to this reason, Mitschka [33] extended the solution obtained by Von Karman to fluids which obeys POWER-LAW relationship and found that for this case the basic flow is not an exact solution of the NavierStokes equations and suitable boundary layer approximation is required. He further proposed generalized Karman similarity transformations for this type of flow problem. Mitschka and Ulbrecht [34], Andersson et al. [35] studied the flow of both shear-thickening and shear-thinning fluids and presented numerical solutions. Santra et al. [36] presented the convective flow of by Cu-water nanofluid inside a channel and concluded that rise in the nanoparticles volume fraction can increase the rate of heat transfer. Zheng et al. [37–42] published several papers considering heat transfer phenomenon of POWER-LAW fluids. Andersson [43] also worked on POWER-LAW fluid flow under the effects of magnetic field. Some of the recent publications on the flow of non-Newtonian POWER-LAW fluid under different physical situations with heat and mass transfer are referred in [44–57].

In this dissertation, the work done by Andersson et al. [35] is extended to investigate the POWER-LAW nanofluid flow and heat transfer over an infinite rotating disk and using variable thermal conductivity. The flow is induced to the rotation of disk and initially no slip conditions are assumed at the boundary. This idea is further extended by introducing magnetohydrodynamics (MHD) slip flow of POWER-LAW nanofluid over the same rotating disk. The governing system which is a set of partial differential equations (PDEs) are first changed into ordinary differential equations (ODEs) using similarity transformation. This system is then solved numerically with MATLAB *bvp4c* code. Two different types of nanofluids, namely Cu-water and Al_2O_3-water are considered in this work. Graphical analysis is presented to study velocity and temperature profiles effected by different physical parameters. No work has been done to study POWER-LAW nanofluid over an infinite rotating

disk using variable thermal conductivity with or without MHD.

The dissertation is arranged as follows: Chapter 2 presents few basic definitions of fluid flow, fundamental concepts of fluid mechanics, heat transfer terminologies, POWER-LAW model for non-Newtonian fluids and the fundamental governing equations of the flow. In Chapter 3 detailed investigation is carried out over a rotating disk for POWER-LAW fluid flow. Chapter 4 presents a comprehensive study for the phenomenon of POWER-LAW nanofluid flow with mass and heat transfer over a rotating disk. In Chapter 5, the study presented in chapter 4 is further extended by including analysis of MHD POWER-LAW nanofluid flow under slip conditions over a rotating disk. Chapter 6 concludes the research work and discuss possible future work.

Chapter 2

PRELIMINARIES

Basic definitions regarding fluid flow, types of fluid flow and basic governing equations regarding the fluid flow, heat transfer and modes of heat transfer are introduced here. In addition an introduction to nanofluids and some of nanofluid's physical parameters are also presented.

2.1   Fluid

A fluid is a particular kind of matter that has the ability to continuously deform itself when shear stress is applied on it. This includes liquids, gases, plasmas and some plastic solids.

2.2   Fluid flow

The phenomenon in which fluid continuously deforms itself is known as fluid flow.

2.3 Steady flow

A flow in which properties of fluid at a particular point remain unchanged with time is known as steady flow. Mathematically speaking

$$\frac{d\gamma}{dt} = 0, \tag{2.3.1}$$

where γ is any fluid property and t is time.

2.4 Unsteady flow

A flow in which fluid at a particular point changes its properties with time is known as unsteady flow. Mathematically it is stated as

$$\frac{d\gamma}{dt} \neq 0. \tag{2.4.1}$$

2.5 Laminar flow

It is a kind of fluid flow in which fluid moves smoothly in parallel layers. The path lines of fluid particles do not cross each other. This flow usually occurs while dealing with low Reynolds number.

2.6 Turbulent flow

It is a kind of fluid flow in which fluid particles continuously changes their direction. This flow occurs with high Reynolds number.

2.7 Compressible flow and incompressible flow

A fluid flow in which the density (ρ) of the fluid remains constant is known as incompressible flow i.e.,

$$\frac{D\rho}{Dt} = 0. \tag{2.7.1}$$

Here, $\frac{D}{Dt}$ denotes the material derivative which is defined as

$$\frac{D}{Dt} = \frac{\partial}{\partial t} + \mathbf{V} \cdot \nabla. \tag{2.7.2}$$

A fluid flow in which the density of fluid varies with time is known as compressible flow i.e.,

$$\frac{D\rho}{Dt} \neq 0. \tag{2.7.3}$$

2.8 Axi-symmetric flow

An axi-symmetric flow is the one in which all the streamlines are positioned symmetrically around the axis. In this flow both pressure term p and the cylindrical velocity components v_r, v_θ, v_z are independent of the angular variable θ.

2.9 Viscosity

Viscosity is a quantity that shows fluid opposition to the deformation or shear stresses and is measured by the coefficient of viscosity, μ. Mathematically it is written as

$$\mu = \frac{\text{shear stress}}{\text{deformation rate}}. \tag{2.9.1}$$

In the above equation μ is **dynamic** or **absolute viscosity**. The other type of viscosity is called as **Kinematic Viscosity**, ν, which is a ratio between dynamic viscosity to density of the fluid and has a following expression

$$\nu = \frac{\mu}{\rho}. \tag{2.9.2}$$

The fluids having non-zero viscosity are known as **Viscous fluids** while those having zero dynamic viscosity are known as **Inviscid fluids**.

2.10   Stress

Stress is a term which is equal to force per unit area. It has two components i.e., shear/tangential stress, normal stress. Mathematical expression of stress is

$$\tau = \frac{F}{A},\tag{2.10.1}$$

where stress term is represented by τ, F represents the applied force and cross sectional area is represented by A.

2.11   Newton's law of viscosity

This law creates a relationship between stress on fluid and the rate of shear strain. In other words, shear stress is proportional (linearly) to velocity gradient. Mathematically it can be written as

$$\tau_{xy} = \mu \frac{du}{dy},\tag{2.11.1}$$

where τ denotes shear stress, μ is coefficient of viscosity and $\frac{du}{dy}$ shows shear strain rate.

2.12   Newtonian fluids

Newtonian fluids are those fluids which obeys Newton's law of viscosity. Most common Newtonian fluids are water, air, gasoline, organic solvents etc.

2.13 Non-newtonian fluids

Fluids having the property that shear stress is not linearly proportional to rate of deformation are called as non-Newtonian fluids. Some of the substances that shows non-Newtonian behavior are ketchup, jams, yogurt, butter, gums, soup solution, cement slurry, blood, saliva etc.

2.14 POWER–LAW model

POWER–LAW model is one of the most common model proposed for non-Newtonian fluids. Mathematical form of this model in unidirectional flow is

$$\tau_{xy} = K \left(\frac{du}{dy}\right)^n. \tag{2.14.1}$$

Here, K denotes consistency index while n is a flow behavior index. We can also write the above equation as

$$\tau_{xy} = \eta \frac{du}{dy}, \tag{2.14.2}$$

where η is the apparent viscosity and is expressed as

$$\eta = K \left[\frac{du}{dy}\right]^{n-1}. \tag{2.14.3}$$

The parameter n decides the nature of fluid behavior. For $n > 1$, (2.14.1) represents the behavior of shear thickening while for $n < 1$, (2.14.1) represents the behavior of shear thinning. When $n = 1$, (2.14.1) becomes same as for Newtonian fluids.

2.15 Mass equation / Continuity equation

Continuity equation is based on law of conservation of mass which states that mass can neither be generated nor demolished but can be converted from one profile to

another inside a control volume. Mathematically it is written as

$$\frac{\partial \rho}{\partial t} + \nabla \cdot (\rho \mathbf{V}) = 0, \qquad (2.15.1)$$

where $\mathbf{V}$ represents velocity vector and ∇ is the differential operator. If density ρ is constant then (2.15.1) becomes

$$\nabla \cdot \mathbf{V} = 0. \qquad (2.15.2)$$

2.16   Momentum equation

Law of conservation of momentum states that total force acting on a particle in fluid is equal to time rate of change of linear momentum.

Momentum equation is derived by generalizing the law of conservation of momentum. Mathematical form of this law is known as Navier-Strokes equation and has the form

$$\rho \frac{D\mathbf{V}}{Dt} = \nabla \cdot \tau + \rho \mathbf{b}. \qquad (2.16.1)$$

Here, τ denote Cauchy stress tensor, $\nabla \cdot \tau$ represent surface forces and $\rho \mathbf{b}$ is body force per unit mass.

2.17   Heat transfer

Heat transfer is a process in which transferring of thermal energy occurs due to temperature difference between the physical systems. There are three different ways of heat transfer, conduction, convection, radiation.

2.17.1   Conduction

The process of heat transfer which occurs because of the molecular collisions is known as conduction. Fourier developed a law known as Fourier's law of heat conduction.

11

Mathematical form of the law is

$$Q = -kA\frac{dT}{dx}, \qquad (2.17.1)$$

where Q is heat flow rate, T shows temperature, A is cross-sectional area, $\frac{dT}{dx}$ is temperature gradient and k is thermal conductivity.

2.17.2 Convection

It is defined as heat transfer in fluids from a part with high temperature to a part where temperature is comparatively low. In convection, Newton's law of cooling governs heat transfer rate with the expression

$$Q = hA(T_s - T_\infty), \qquad (2.17.2)$$

where h represent coefficient of convection, T_s is temperature of surface and T_∞ is temperature of the outside environment.

2.17.3 Radiation

Radiation occurs by photons of light or waves emitted from a surface volume. Radiation can happen in vacuum also. Stefan-Boltzmann law is used to calculate the amount transfer through radiation. Mathematically

$$Q = \sigma \cdot T^4, \qquad (2.17.3)$$

where σ denotes Stefan-Boltzmann's constant.

2.18 Energy equation

This equation is formed by generalizing the first law of thermodynamics which ensures that rate of change of fluid's energy inside a control volume is equals to rate

12

of work done due to body or surface forces and rate of heat addition. The governing equation which includes energy conservation can be composed as

$$\rho C_p \frac{D\mathbf{T}}{Dt} = \nabla \cdot (k\nabla T) + f \cdot \mathbf{V}. \tag{2.18.1}$$

In the above expression, C_p denote specific heat at a constant temperature and f is surface or body force.

2.19 Magnetohydrodynamics (MHD)

Branch of engineering in which behavior of magnetic field in electrically conducting fields is studied is known as Magnetohydrodynamics. Combination of equations of motion and Maxwells equation of electromagnetism results in the set of equations which represents MHD flow. The momentum equation (2.16.1) with electromagnetic force term for MHD fluid flow is

$$\rho \frac{D\mathbf{V}}{Dt} = \nabla \cdot \tau + (\mathbf{J} \ \mathbf{x} \ \mathbf{B}), \tag{2.19.1}$$

where $\mathbf{J}$ shows density of current and $\mathbf{B}$ is total magnetic field which has following expression

$$\mathbf{B} = \mathbf{B} + \mathbf{B}_1, \tag{2.19.2}$$

where $\mathbf{B}_1$ is the induced magnetic field. In this thesis, we considered that $\mathbf{B}_1$ as very small in comparison with external magnetic field and thus it can be ignored. This is justified for MHD flow with small Reynolds number. By Ohms law, $\mathbf{J}$ is given as

$$\mathbf{J} = \sigma(\mathbf{E} + \mathbf{V} \times \mathbf{B}), \tag{2.19.3}$$

where σ is electrical conductivity and $\mathbf{E}$ is electrical field. After simplification equation 2.19.3 becomes

$$\mathbf{J} \times \mathbf{B} = \sigma \mathbf{B}^2 \mathbf{V}. \qquad (2.19.4)$$

Using equation 2.19.3, momentum equation 2.19.1 becomes

$$\rho \frac{D\mathbf{V}}{Dt} = \nabla \cdot \tau + \sigma \mathbf{B}^2 \mathbf{V}. \qquad (2.19.5)$$

2.20 Boundary conditions

It is the set of conditions which must be satisfied at a region in which a system of differential equations has to be solved.

2.20.1 No-slip condition

No–slip boundary condition tells us that fluid which is flowing over a solid surface have zero velocity relative to the boundary.

2.20.2 Slip condition

Slip boundary condition tells us that velocity of fluid at surface is proportional to shear stress at surface.

2.21 Boundary layer

The layer of fluid over the surface where viscosity effects are very significant is called a boundary layer. Viscosity is maximum near the surface and it decreases gradually as fluid moves away from the surface. On boundary layer, the velocity of fluid

particles is approximately the same as that of velocity of fluid particles outside the boundary layer. This velocity is called **free stream velocity**.

2.22 Boundary layer thickness

It is a distance from surface to the fluid layer which attains a free stream velocity.

2.23 Skin friction coefficient

Measure of resistance between the solid surface and fluid is known as skin friction coefficient. It is defined as

$$C_f = \frac{\tau_w}{\rho U_w{}^2}. \tag{2.23.1}$$

In the above relation, τ_w is total wall shear stress while U_w is surface velocity where τ_w has the expression

$$\tau_w = \sqrt{\tau_{zr}^2 + \tau_{z\theta}{}^2}, \tag{2.23.2}$$

in which

$$\tau_{zr} = \mu_{nf} \frac{\partial v_1}{\partial z}\big|_{z=0}, \quad \tau_{z\theta} = \mu_{nf} \frac{\partial v_2}{\partial z}\big|_{z=0}. \tag{2.23.3}$$

2.24 Nusselt number

Nusselt number is defined as

$$Nu = \frac{\text{convective heat transfer}}{\text{conductive heat transfer}} = \frac{hL}{k}. \tag{2.24.1}$$

In the above relation, h represents fluid's convective heat transfer coefficient, L denotes characteristic length and k is thermal conductivity of fluid. In this thesis, we are taking Nusselt number as

$$Nu_r = \frac{rq_w}{k_f(T_w - T_\infty)}, \tag{2.24.2}$$

with wall heat flux as

$$q_w|_{z=0} = -k_{nf}\frac{\partial T}{\partial z}|_{z=0}. \qquad (2.24.3)$$

2.25 Reynolds number

Reynold number is defined as

$$Re = \frac{\text{inertial force}}{\text{viscous force}} = \frac{uL}{\nu}, \qquad (2.25.1)$$

where u gives bulk velocity, L is a typical length scale in the system.

2.26 Prandtl number

Prandtl number is defined as

$$Pr = \frac{\text{momentum diffusivity}}{\text{thermal diffusivity}} = \frac{\nu}{\alpha} = \frac{C_p\mu}{k}. \qquad (2.26.1)$$

2.27 Hartmann number

It is defined as

$$Ha = \frac{\text{electromagnetic force}}{\text{viscous force}} = BL\sqrt{\frac{\sigma}{\mu}}. \qquad (2.27.1)$$

2.28 Similarity transformation

It is technique used in Mathematics which reduces the number of independent variables in a system of partial differential equations (PDEs) and transform it to a system of ordinary differential equations (ODEs).

2.29 Nanofluids

Nanofluids is a special class of fluids with enhanced thermal conductivity. Nanofluids contains base fluid (water, oil, ethynol, etc) in which nanometer-sized particles (1-100 nm) (named as nanoparticles) are suspended. Some common nanoparticles used to produce nanofluids are formed by metals (Cu, Al, Ag), oxides (Al_2O_3, CuO), carbides (SiC, TiC) and carbon nanotubes. Nanofluids can be used in many applications of heat transfer for example fuel cells, heat exchanger, chiller and biomedicine.

2.30 Physical parameters of nanofluid

Some of the physical parameters used in the discussion of nanofluids are mentioned below

2.30.1 Viscosity

Viscosity of nanofluid is given by Brinkman [58] as

$$\mu_{nf} = \frac{\mu_f}{(1-\phi)^{2.5}}. \tag{2.30.1}$$

In the above equation, ϕ gives nanoparticle volume fraction coefficient while μ_f denotes dynamic viscosity of base fluid.

2.30.2 Density

Density of nanofluid is given by Khanafer et al. [59] as

$$\rho_{nf} = (1-\phi)\rho_f + \phi\rho_s, \tag{2.30.2}$$

where ρ_f and ρ_s are density of base fluid and solid nanoparticles respectively.

2.30.3   Specific heat

Specific heat of nanofluid $(C_p)_{nf}$ has the relation given by Khanafer et al. [59] as

$$(\rho C_p)_{nf} = (1 - \phi)(\rho C_p)_f + \phi(\rho C_p)_s, \qquad (2.30.3)$$

where $(C_p)_s$ denotes specific heat of the solid nanoparticle and $(C_p)_f$ denotes specific heat capacity of base fluid.

2.30.4   Thermal conductivity

It is given by Maxwell [1] as

$$k_{nf} = k_f \left[\frac{k_s + 2k_f - 2\phi(k_f - k_s)}{k_s + 2k_f + \phi(k_f - k_s)} \right], \qquad (2.30.4)$$

where k_s and k_f denotes thermal conductivity of both nanoparticle and base fluid.

2.30.5   Electrical conductivity

Electrical conductivity of nanofluid is given by Cebeci [60] as

$$\sigma_{nf} = \sigma_f \left[1 + \frac{3\left(\frac{\sigma_s}{\sigma_f} - 1\right)\phi}{\left(\frac{\sigma_s}{\sigma_f} + 2\right) - \left(\frac{\sigma_s}{\sigma_f} - 1\right)\phi} \right]. \qquad (2.30.5)$$

In the above equation, σ_s and σ_f denotes electrical conductivity of nanoparticle and base fluid respectively.

Chapter 3

NUMERICAL STUDY OF POWER-LAW FLUID OVER A REVOLVING SURFACE

This chapter covers a review of the work done by Andersson et al. [35]. It describes the laminar, steady and axi-symmetric flow of a POWER-LAW fluid over a rotating disk. The governing PDEs are first modeled and then reduced into a set of ODEs with the help of similarity transformations. Using MATLAB bulit-in solver $bvp4c$ the new equations are then solved numerically. Results are then described in the form of tables and graphs, influence of POWER-LAW index n on radial, tangential and axial flow is examined. Section 3.1 and section 3.2 of this chapter includes the mathematical formation of problem. Section 3.3 describes the numerical method to obtain the solution. Numerical results obtained with the help of $bvp4c$ solver are presented and discussed in section 3.4.

3.1 Mathematical model

Assume an incompressible non-Newtonian fluid which covers the space over an infinite rotating disk. The motion of fluid is bounded to the half space located above the disk. The steady flow is considered axi-symmetric and the disk is rotating uniformly and smoothly with angular velocity Ω about z-axis. The geometry of the flow can be seen from the figure given below.
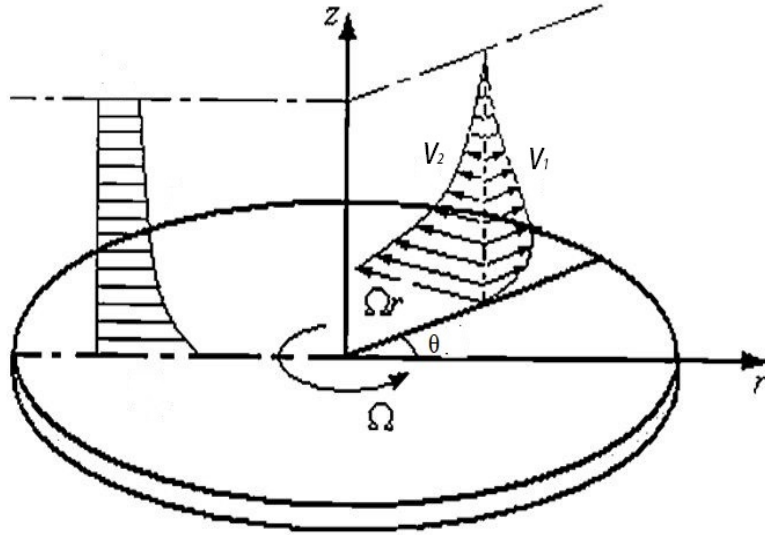

Figure 3.1 – Flow geometry.

The model considered for modeling of the flow is Ostwald-de-Waele POWER-LAW i.e.,

$$\tau_{ij} = 2\mu D = 2K(D_{ij}D_{ij})^{(n-1)/2}D, \tag{3.1.1}$$

where n, K and D denotes the POWER-LAW index, consistency coefficient and the deformation rate, respectively. The tensor components of rate-of-strain in the axi-symmetric flow simplify to

$$D_{rr} = \frac{\partial v_1}{\partial r}, \qquad D_{\varphi\varphi} = \frac{v_1}{r}, \tag{3.1.2}$$

$$D_{zz} = \frac{\partial v_3}{\partial z}, \qquad D_{r\varphi} = D_{\varphi r} = \frac{1}{2} r \frac{\partial}{\partial r}\left(\frac{v_2}{r}\right), \tag{3.1.3}$$

$$D_{\varphi z} = D_{z\varphi} = \frac{1}{2}\frac{\partial v_2}{\partial z}, \qquad D_{rz} = D_{zr} = \frac{1}{2}\left(\frac{\partial v_1}{\partial z} + \frac{\partial v_3}{\partial r}\right). \tag{3.1.4}$$

The viscosity function take the form

$$\mu = K\left(2\left(\frac{\partial v_1}{\partial r}\right)^2 + 2\left(\frac{v_1}{r}\right)^2 + 2\left(\frac{\partial v_3}{\partial z}\right)^2 + \left[r\frac{\partial}{\partial r}\left(\frac{v_2}{r}\right)\right]^2 + \left(\frac{\partial v_2}{\partial z}\right)^2 + \left(\frac{\partial v_1}{\partial z} + \frac{\partial v_3}{\partial r}\right)^2\right)^{(n-1)/2}. \tag{3.1.5}$$

The constitutive equations for conservation of mass and momentum now can be written as

$$\frac{\partial v_1}{\partial r} + \frac{v_1}{r} + \frac{\partial v_3}{\partial z} = 0, \tag{3.1.6}$$

$$\rho\left(v_1\frac{\partial v_1}{\partial r} + v_3\frac{\partial v_1}{\partial z} - \frac{v_2{}^2}{r}\right) = -\frac{\partial p}{\partial r} + \frac{1}{r}\frac{\partial(r\tau_{rr})}{\partial r} + \frac{\partial(\tau_{zr})}{\partial z} - \frac{\tau_{\varphi\varphi}}{r}, \tag{3.1.7}$$

$$\rho\left(v_1\frac{\partial v_2}{\partial r} + v_3\frac{\partial v_2}{\partial z} + \frac{v_1 v_2}{r}\right) = \frac{1}{r^2}\frac{\partial(r^2\tau_{r\varphi})}{\partial r} + \frac{\partial(\tau_{z\varphi})}{\partial z} + \frac{\tau_{\varphi r} - \tau_{r\varphi}}{r}, \tag{3.1.8}$$

$$\rho\left(v_1\frac{\partial v_3}{\partial r} + v_3\frac{\partial v_3}{\partial z}\right) = -\frac{\partial p}{\partial z} + \frac{1}{r}\frac{\partial(r\tau_{rz})}{\partial r} + \frac{\partial\tau_{zz}}{\partial z}. \tag{3.1.9}$$

where the components of velocity in radial, tangential and axial direction are denoted by v_1, v_2 and v_3 respectively. Following assumptions are considered while writing the above equations

1) The system is taken as time independent

$$\frac{\partial}{\partial t} = 0.$$

2) Symmetry occurs about the axis of rotation

$$\frac{\partial}{\partial \varphi} = 0.$$

In order to develop dimension free system, following non-dimensional variables are introduced

$$v_1{}^* = \frac{v_1}{U}, \qquad v_2{}^* = \frac{v_2}{U}, \qquad v_3{}^* = \frac{v_3}{U} Re^{1/(n+1)}, \qquad (3.1.10)$$

$$p^* = \frac{p}{\rho U^2}, \qquad r^* = \frac{r}{R}, \qquad z^* = \frac{z}{R} Re^{1/(n+1)}, \qquad (3.1.11)$$

where Re represents the generalized Reynolds number which is equal to

$$Re \equiv \frac{\rho U^{2-n} R^n}{K} \qquad (3.1.12)$$

while U and R are appropriate scales for velocity and length in (r,φ) - plane.

During boundary layer approximation we can simplify the resulting PDEs by taking the limit Re $\rightarrow \infty$ so that all the terms which includes Re in denominator becomes zero and we easily form a boundary layer model having equations

$$\rho \left(v_1 \frac{\partial v_1}{\partial r} + v_3 \frac{\partial v_1}{\partial z} - \frac{v_2{}^2}{r} \right) = -\frac{\partial p}{\partial r} + \frac{\partial}{\partial z} \left(\mu \frac{\partial v_1}{\partial z} \right), \qquad (3.1.13)$$

$$\rho \left(v_1 \frac{\partial v_2}{\partial r} + v_3 \frac{\partial v_2}{\partial z} + \frac{v_1 v_2}{r} \right) = \frac{\partial}{\partial z} \left(\mu \frac{\partial v_2}{\partial z} \right), \qquad (3.1.14)$$

$$\frac{\partial p}{\partial z} = 0. \qquad (3.1.15)$$

The equation (3.1.15) guarantee that the external pressure passes through the boundary layer which means that across the boundary layer pressure term remains constant. The μ (now known as simplified viscosity function) changes to

$$\mu = K \left(\left(\frac{\partial v_1}{\partial z} \right)^2 + \left(\frac{\partial v_2}{\partial z} \right)^2 \right)^{(n-1)/2}. \qquad (3.1.16)$$

The boundary conditions are

$$v_1 = 0 = v_3 \text{ with } v_2 = \Omega r \text{ at } z = 0, \qquad v_1 = 0 = v_2 \text{ as } z \to \infty, \qquad (3.1.17)$$

while for the limiting case of large z, axial velocity (v_3) approach some unknown constant.

3.2 Similarity transformation

The governing PDEs are now diminished to the one produced by Mitschka [33] in his work. Therefore, now we can introduce dimensionless similarity variable η as considered in [33]

$$\eta = z \left(\frac{\Omega^{2-n}}{K/\rho} \right)^{1/(n+1)} \cdot r^{(1-n)/(1+n)}. \qquad (3.2.1)$$

The velocity field is

$$v_1 = r\Omega F(\eta), \qquad v_2 = r\Omega G(\eta), \qquad (3.2.2)$$

$$v_3 = r^{(n-1)/(1+n)} \left(\frac{\Omega^{1-2n}}{K/\rho} \right)^{\frac{-1}{n+1}} H(\eta). \qquad (3.2.3)$$

In agreement with Von Karman's [32] original transformation, we considered pressure as a function of z only. The set of equations (3.1.13)-(3.1.14) along with the continuity equation now transform into a system of ODEs

$$H' = -2F - \frac{1-n}{1+n}\eta F', \qquad (3.2.4)$$

$$F^2 - G^2 + \left(H + \frac{1-n}{1+n}\eta F \right) F' = \left[\left(F'^2 + G'^2 \right)^{(n-1)/2} F' \right]', \qquad (3.2.5)$$

$$2FG + \left(H + \frac{1-n}{1+n}\eta F \right) F' = \left[\left(F'^2 + G'^2 \right)^{(n-1)/2} G' \right]', \qquad (3.2.6)$$

where $'$ is a derivative of functions with respect to η. Also equations (3.1.17) reduced to

$$F = 0, \ G = 1, \ H = 0 \text{ at } \eta = 0, \qquad F = 0, \ G = 0 \text{ at } \eta \to \infty. \qquad (3.2.7)$$

23

The first boundary condition assure impermeability at the disk and no-slip condition while second boundary condition tell that radial and azimuthal motion dissipate as the distance from the disk increases.

3.3 Method of solution

The transformed BVP (3.2.4)-(3.2.6) with conditions given in (3.2.7) is now converted to initial value problem (IVP) of first order having dependent variables y_1, y_2, y_3, y_4 and y_5 such that $y_1 = F$, $y_2 = F'$, $y_3 = G$, $y_4 = G'$, and $y_5 = H$. Denote

$$J = \left(y_2^2 + y_4^2\right)^{\frac{1-n}{2}}, \tag{3.3.1}$$

$$K = \left(y_2^2 + y_4^2\right)^{-1}, \tag{3.3.2}$$

$$L = y_5 + \frac{1-n}{1+n}\eta y_1, \tag{3.3.3}$$

$$M = y_1^2 - y_3^2 + \left(y_5 + \frac{1-n}{1+n}\eta y_1\right)y_2, \tag{3.3.4}$$

$$N = 2y_1y_3 + \left(y_5 + \frac{1-n}{1+n}\eta y_1\right)y_4. \tag{3.3.5}$$

We can write this system of first order five coupled equations as

$$y_1' = y_2, \tag{3.3.6}$$

$$y_2' = \frac{1}{n}J\left[M\left(1 + (n-1)Ky_4^2\right) - (n-1)KNy_2y_4\right], \tag{3.3.7}$$

$$y_3' = y_4, \tag{3.3.8}$$

$$y_4' = \frac{1}{n}J\left[N\left(1 + (n-1)Ky_2^2\right) - (n-1)KMy_2y_4\right], \tag{3.3.9}$$

$$y_5' = -2y_1 - \frac{1-n}{1+n}\eta y_2, \tag{3.3.10}$$

Similarly the boundary conditions 3.2.7 changes to

$$y_1 = 0, \; y_3 = 1, \; y_5 = 0 \text{ at } z = 0, \qquad y_1 = 0, \; y_3 = 0 \text{ as } \eta \to \infty. \tag{3.3.11}$$

24

3.4 Numerical results and discussion

Numerical results for equations (3.3.6)-(3.3.10) along with their boundary conditions (3.3.11) are obtained for different values of POWER-LAW index or flow behavior index n via MATLAB built-in solver $bvp4c$ with variable step size. We have compared our outcomes with Andersson et al. [35] and this comparison is presented in Table 3.1. We can see that results are found to be in a good agreement.

Table 3.1 – Comparison between computational results of present calculations and results of Andersson et al. [35].

	$F'(0)$		$-G'(0)$		$-H(\infty)$	
n	Andersson [35]	Present	Andersson [35]	Present	Andersson [35]	Present
1.7	0.537	0.53644	0.600	0.60092	0.633	0.63356
1.3	0.522	0.52149	0.603	0.60345	0.735	0.73591
1.0	0.510	0.51020	0.616	0.61590	0.883	0.88173
0.9	0.507	0.50686	0.624	0.62428	0.969	0.96740
0.8	0.504	0.50391	0.636	0.63618	1.089	1.08118

The results shown in Figure 3.2 and Figure 3.3 are for shear thickening fluids ($n > 1$) and exhibit same characteristics as for Newtonian case(given in Figure 3.4. Rotation of the disk generates a centrifugal force which causes a radial outward flow represented by the curve F in the graph. In order to satisfy Newton's third law motion, the axial inflow $-H$ is generated towards the disk. The peak of curve representing F is slightly affected due to variations in n. The shear driven motion G in tangential direction also decline quickly with the distance η from the disk.

The most noticeable effect in the graphs is thinning of boundary layer monotonically with the increasing values of n. To compensate total mass flow in radial direction the effect of thinning of boundary layer results in minimizing of axial inflow

$(-H)$.

This axial inflow $(-H)$ can be calculated by direct integration of equation (3.2.4)

$$- H^{'}(\infty) = 2 \int_0^\infty F d\eta + \frac{1-n}{1+n} \int_0^\infty F^{'}\eta \; d\eta. \qquad (3.4.1)$$

This decrease in boundary layer thickness with the increasing parameter n is due to the reduction of the value of viscosity function J^{-1}, that can be defined from equation (3.3.1).
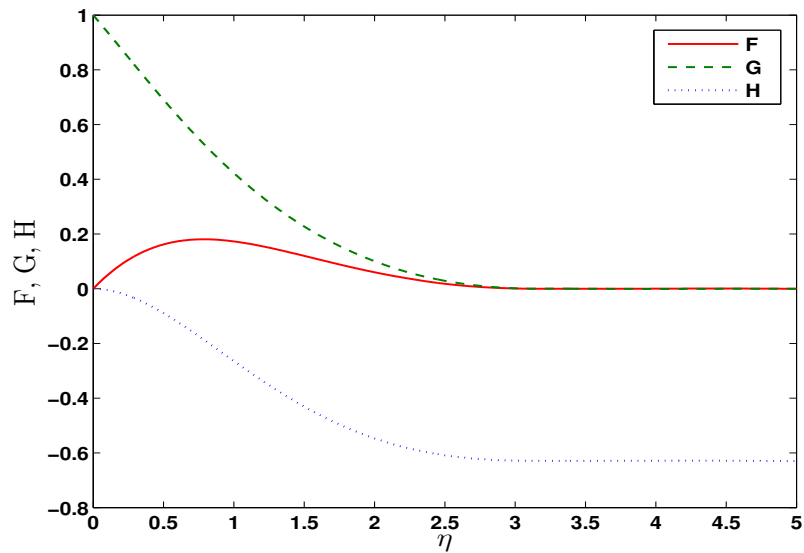

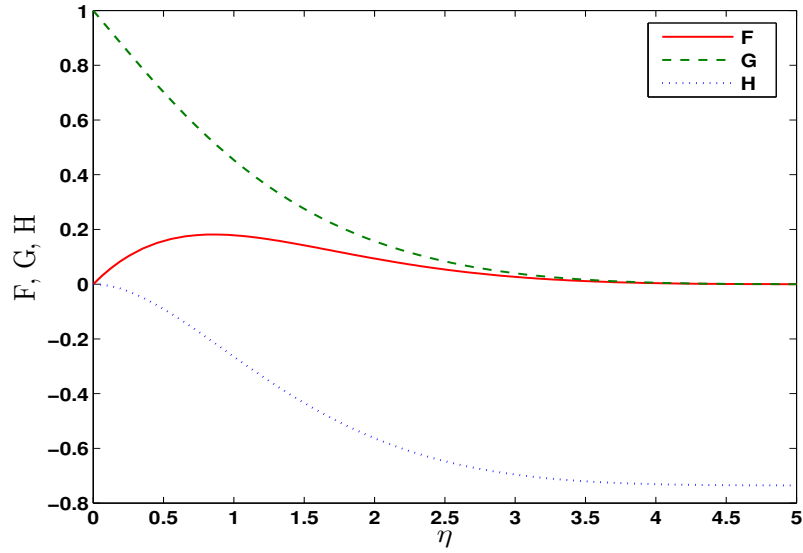Figure 3.2 – Present lines for the components of velocity of a fluid when n = 1.7.

Figure 3.3 – Present lines for the components of velocity of a fluid when n = 1.3.
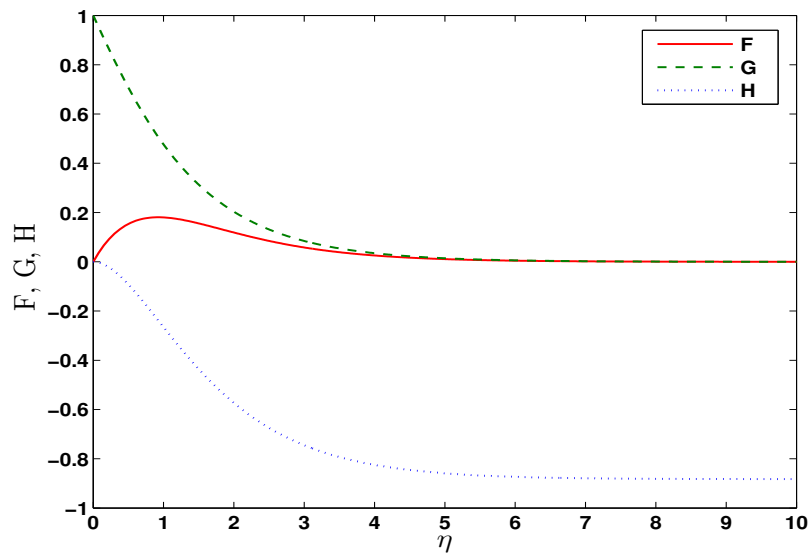
Figure 3.4 – Present lines for the components of velocity of a fluid when n = 1.0.

In Figures 3.5 - 3.7 the behavior of shear thinning fluids ($n < 1$) are presented. Near the disk, motion of the fluid is only slightly affected due to variation in n. Radial velocity profile F stays approximately the same as in Newtonian case (from

Figure 3.4) but the shear driven motion G, which is parallel to the disk motion, infiltrate more into curve of F. This results in the thickening of boundary layer that is due to the increase in viscosity function 3.3.1. This effect give rise to an enhanced inflow $-H$ in axial direction.

For highly shear thinning fluids $(n < 0.5)$, it is difficult to determine the inflow $-H(\infty)$ because for large η-values the axial inflow $-H$ fails to approach an asymptotic limit.
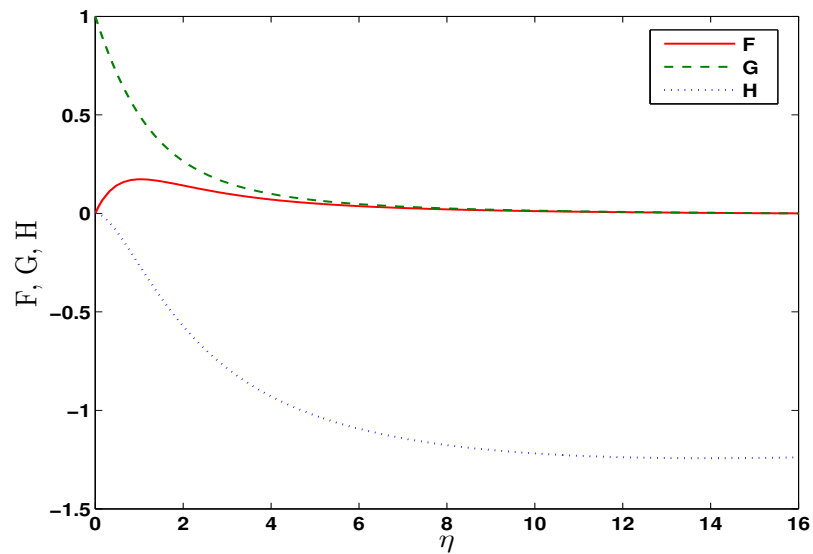
Figure 3.5 – Present lines for the components of velocity of a fluid when n = 0.6.
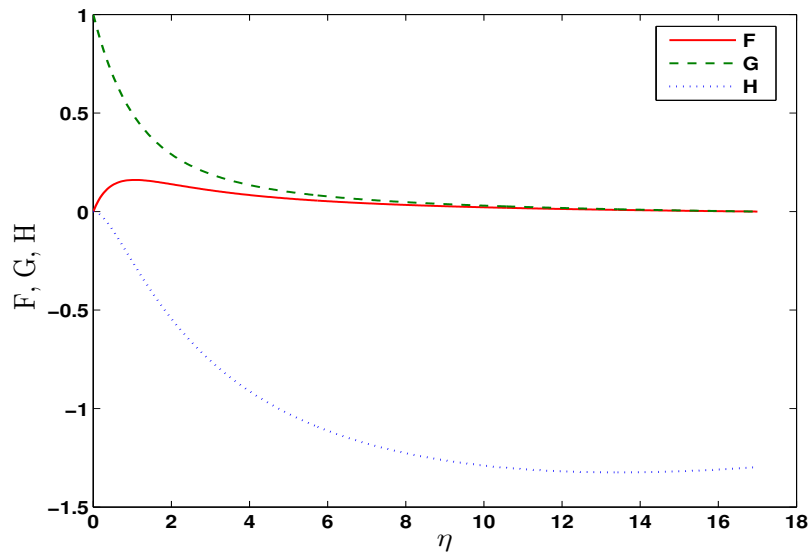
Figure 3.6 – Present lines for the components of velocity of a fluid when n = 0.4.
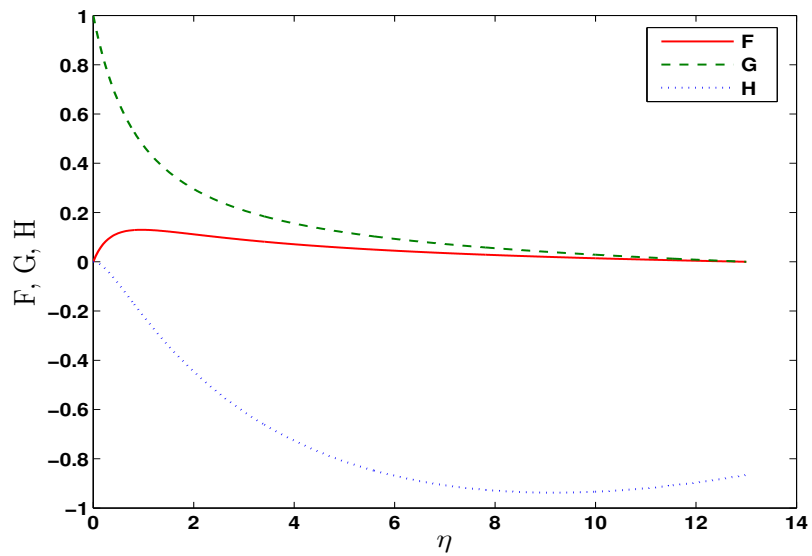
Figure 3.7 – Present lines for the components of velocity of a fluid when n = 0.2.

29

Chapter 4

NUMERICAL INVESTIGATION FOR FLOW OF POWER-LAW NANOFLUID OVER AN INFINITE ROTATING DISK WITH HEAT TRANSFER

This chapter extends the model presented by Andersson et al. [35] for nanofluid flow. The current work deals with the POWER-LAW nanofluid flow over an infinite rotating disk. Variation of thermal conductivity due to velocity gradient is also taken into account as suggested in [25]. Effect of variations in parameters on velocity and thermal profiles are analyzed both numerically and graphically using MATLAB built-in solver *bvp4c*.Both sections 4.1 and 4.2 deals with the mathematical formulation. Section 4.3 is about the details of numerical method that we used for the numerical computations and section 4.4 deals with both numerical and graphical results along with their discussions.

4.1 Mathematical model

Assume an incompressible, 3D axi-symmetric, steady and laminar fluid flow over an infinite rotating disk with heat transfer. The disk has constant angular velocity Ω. The geometry of flow can be seen from the figure given below.
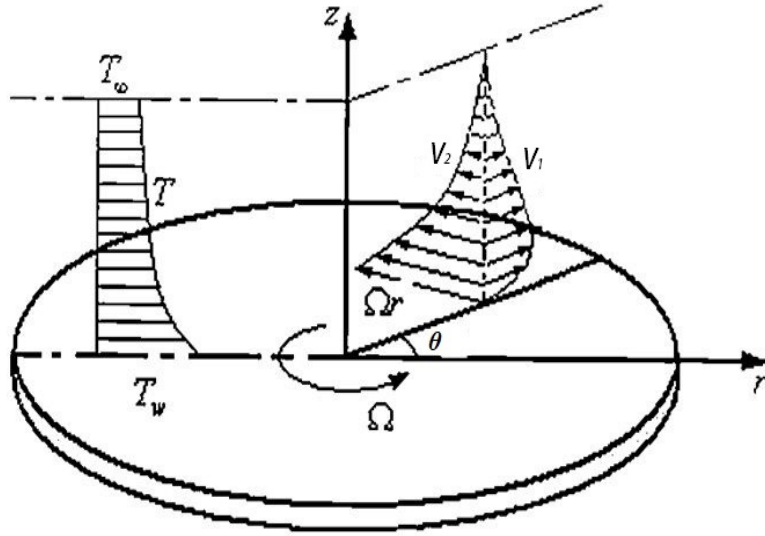
Figure 4.1 – Flow geometry.

The fluid under consideration is a POWER-LAW nanofluid which is incompressible and follow the Ostwald-de Waele POWER-LAW model

$$\tau_{ij} = 2\mu_{nf}D = 2K(D_{ij}D_{ij})^{(n-1)/2}D, \qquad (4.1.1)$$

where μ_{nf} represents the viscosity of nanofluid. The flow is restricted to the half space $z > 0$. The system is considered to be time independent and symmetry occurs over axis of rotation. At the disk the temperature is taken as constant T_w while outside the boundary layer the fluid maintains uniform temperature T_∞. Neglecting all the body forces and under boundary layer approximation, constitutive equations of mass, momentum and energy conservation are given below

$$\frac{\partial v_1}{\partial r} + \frac{v_1}{r} + \frac{\partial v_3}{\partial z} = 0, \qquad (4.1.2)$$

31

$$\rho_{nf}\left(v_1\frac{\partial v_1}{\partial r}+v_3\frac{\partial v_1}{\partial z}-\frac{v_2{}^2}{r}\right)=\frac{\partial}{\partial z}\left(\mu_{nf}\frac{\partial v_1}{\partial z}\right),\tag{4.1.3}$$

$$\rho_{nf}\left(v_1\frac{\partial v_2}{\partial r}+v_3\frac{\partial v_2}{\partial z}+\frac{v_1v_2}{r}\right)=\frac{\partial}{\partial z}\left(\mu_{nf}\frac{\partial v_2}{\partial z}\right),\tag{4.1.4}$$

$$\frac{\partial p}{\partial z}=0,\tag{4.1.5}$$

$$(\rho_{C_p})_{nf}\left(v_1\frac{\partial T}{\partial r}+v_3\frac{\partial T}{\partial z}\right)=\frac{\partial}{\partial z}\left(k_{nf}(T)\frac{\partial T}{\partial z}\right).\tag{4.1.6}$$

The viscosity function is

$$\mu_{nf}=\frac{K}{(1-\phi)^{2.5}}\left(\left(\frac{\partial v_1}{\partial z}\right)^2+\left(\frac{\partial v_2}{\partial z}\right)^2\right)^{\frac{n-1}{2}}.\tag{4.1.7}$$

In equation (4.1.6), k_{nf} is the variable thermal conductivity of nanofluid.

Above boundary layer problem has following boundary conditions

$$v_1=0=v_3 \text{ with } v_2=\Omega r,\ T=T_w \text{ at } z=0,\qquad v_1=0=v_2,\ T\to T_\infty \text{ as } z\to\infty,\tag{4.1.8}$$

while for the limiting case of large z, axial velocity (v_3) approach some unknown constant.

The thermal conductivity k_{nf} of the nanofluid is assumed to vary with velocity gradients i.e.,

$$k_{nf}(T)=k_{nf}^*\left(\left(\frac{\partial v_1}{\partial z}\right)^2+\left(\frac{\partial v_2}{\partial z}\right)^2\right)^{\frac{n-1}{2}}.\tag{4.1.9}$$

Here k_{nf}^* is constant nanofluid's thermal conductivity and has the expression

$$k_{nf}^*=k_f\left[\frac{k_s+2k_f-2\phi(k_f-k_s)}{k_s+2k_f+\phi(k_f-k_s)}\right].\tag{4.1.10}$$

4.2   Similarity transformation

At this stage, we are going to use Mitschka's [33] similarity variable which is denoted by η and has the following expression

$$\eta=z\,r^{(1-n)/(1+n)}\left(\frac{\Omega^{2-n}}{K/\rho}\right)^{1/(n+1)}.\tag{4.2.1}$$

Let

$$v_1 = r\Omega F(\eta), \qquad v_2 = r\Omega G(\eta), \tag{4.2.2}$$

$$v_3 = r^{(n-1)/(1+n)}\left(\frac{\Omega^{1-2n}}{K/\rho}\right)^{\frac{-1}{n+1}} H(\eta), \qquad \theta(\eta) = \frac{T - T_\infty}{T_w - T_\infty}. \tag{4.2.3}$$

For details see [32–35]. By introducing these transformations the above boundary layer equations (4.1.2)-(4.1.6) transform into the following ODEs.

$$H' = -2F - \frac{1-n}{1+n}\eta F', \tag{4.2.4}$$

$$\left(1 - \phi + \frac{\rho_s}{\rho_f}\phi\right)\left[F^2 - G^2 + \left(H + \frac{1-n}{1+n}\eta F\right)F'\right] = \frac{1}{(1-\phi)^{2.5}}\left[\left(F'^2 + G'^2\right)^{(n-1)/2} F'\right]', \tag{4.2.5}$$

$$\left(1 - \phi + \frac{\rho_s}{\rho_f}\phi\right)\left[2FG + \left(H + \frac{1-n}{1+n}\eta F\right)G'\right] = \frac{1}{(1-\phi)^{2.5}}\left[\left(F'^2 + G'^2\right)^{(n-1)/2} G'\right]', \tag{4.2.6}$$

$$\left[H + \left(\frac{1-n}{1+n}\right)F\eta\right]\theta'\left(\frac{\left(1 - \phi + \frac{(\rho C_p)_s}{(\rho C_p)_f}\phi\right)}{\left(\frac{k_s + 2k_f - 2\phi(k_f - k_s)}{k_s + 2k_f + \phi(k_f - k_s)}\right)}\right) = \frac{1}{Pr}\left[\left(F'^2 + G'^2\right)^{\frac{n-1}{2}}\theta'\right]', \tag{4.2.7}$$

where Pr is Prandtl number. According to the similarity transformation proposed by Von Karman in 1921, p is the function of z only i.e., $\frac{\partial p}{\partial r} = 0$. Also equation (4.1.5) suggests that the pressure p stays constant over the boundary layer. This suggests that the pressure term is a true constant.

The conditions in (4.1.8) changes to

$$F = 0, \ G = 1, \ H = 0, \ \theta = 1 \text{ at } \eta = 0, \qquad F = 0, \ G = 0, \ \theta = 0 \text{ as } \eta \to \infty. \tag{4.2.8}$$

Here the main quantities of great interest are Nusselt number and skin friction coefficient. Using the above similarities, the skin friction coefficient (2.23.1) and Nusselt number (2.24.2) becomes

$$C_f Re_r^{1/n+1} = \frac{[F'(0)^2 + G'(0)^2]^{n/2}}{(1-\phi)^{2.5}}. \tag{4.2.9}$$

33

$$Nu_r Re_r^{-1/n+1} = \frac{-k_{nf}}{k_f}\theta'(0). \qquad (4.2.10)$$

Here Re_r is the local Reynold's number.

4.3 Numerical method for solution

We can transform the above BVP (4.2.4)-(4.2.7) to initial value problem (IVP) having first order with dependent variables y_1, y_2, y_3, y_4, y_5, y_6 and y_7 such that $y_1 = F$, $y_2 = F'$, $y_3 = G$, $y_4 = G'$, $y_5 = H$, $y_6 = \theta$ and $y_7 = \theta'$. Denote

$$J = \left(y_2^2 + y_4^2\right)^{\frac{1-n}{2}}, \qquad (4.3.1)$$

$$K = \left(y_2^2 + y_4^2\right)^{-1}, \qquad (4.3.2)$$

$$L = y_5 + \frac{1-n}{1+n}\eta y_1, \qquad (4.3.3)$$

$$M = y_1^2 - y_3^2 + \left(y_5 + \frac{1-n}{1+n}\eta y_1\right)y_2, \qquad (4.3.4)$$

$$N = 2y_1 y_3 + \left(y_5 + \frac{1-n}{1+n}\eta y_1\right)y_4. \qquad (4.3.5)$$

Then we can write coupled seven equations of first order as

$$y_1' = y_2, \qquad (4.3.6)$$

$$y_2' = \mathbf{U}\frac{1}{n}J\left[M\left(1 + (n-1)Ky_4^2\right) - (n-1)KNy_2y_4\right], \qquad (4.3.7)$$

$$y_3' = y_4, \qquad (4.3.8)$$

$$y_4' = \mathbf{U}\frac{1}{n}J\left[N\left(1 + (n-1)Ky_2^2\right) - (n-1)KMy_2y_4\right], \qquad (4.3.9)$$

$$y_5' = -2y_1 - \frac{1-n}{1+n}\eta y_2, \qquad (4.3.10)$$

34

$$y_6^{'} = y_7, \tag{4.3.11}$$

$$y_7^{'} = Jy_7 \left[L \left(Pr\mathbf{Q} - \frac{(n-1)}{n}\mathbf{U} \right) - \left(\frac{n-1}{n} \right) \mathbf{U}K \left(2y_1y_3y_4 + y_1{}^2y_2 - y_2y_3{}^2 \right) \right], \tag{4.3.12}$$

where $\mathbf{Q}$ and $\mathbf{U}$ has the expressions

$$\mathbf{Q} \equiv \frac{\left(1 - \phi + \frac{(\rho C_p)_s}{(\rho C_p)_f}\phi \right)}{\left(\frac{k_s + 2k_f - 2\phi(k_f - k_s)}{k_s + 2k_f + \phi(k_f - k_s)} \right)}, \tag{4.3.13}$$

$$\mathbf{U} \equiv \left[(1 - \phi)^{2.5}(1 - \phi + \frac{\rho_s}{\rho_f}\phi) \right]. \tag{4.3.14}$$

Similarly the equation(4.2.8) changes to

$$y_1 = 0, \ y_3 = 1, \ y_5 = 0, \ y_6 = 1 \text{ at } z = 0, \qquad y_1 = 0, \ y_3 = 0, \ y_6 = 0 \text{ as } \eta \to \infty. \tag{4.3.15}$$

4.3.1 Verification of numerical results

We will first compare the current results with Andersson et al. [35], Ming et al. [25] and Mitschka (1965) [34] for different values of POWER-LAW index n by assuming $Pr = 6.2$ and $\phi = 0$. The comparisons are given in Tables 4.1, 4.2 and 4.3 and they clearly displays that our results are in a good correspondence with others. A good comparison suggest that the results produced using the above mentioned scheme are valid.

Table 4.1 – Comparison between present calculation of $F^{'}(0)$ and results of Andersson et al. [35], Ming et al. [25] and Mitschka (1965) [34].

n	$F^{'}(0)$			
	Mitschka [34]	Andersson [35]	Ming [25]	Present
2.0	-	0.547	0.54676	0.54694
1.7	-	0.537	0.53664	0.53663
1.5	0.529	0.529	0.52919	0.52908
1.3	0.521	0.522	0.52150	0.52148
1.0	0.510	0.510	0.51021	0.51022
0.8	0.504	0.504	0.50381	0.50384
0.5	0.501	0.501	0.50058	0.49005

Table 4.2 – Comparison between present calculation of $-G^{'}(0)$ and results of Andersson et al. [35], Ming et al. [25] and Mitschka (1965) [34].

n	$-G^{'}(0)$			
	Mitschka [34]	Andersson [35]	Ming [25]	Present
2.0	-	0.603	0.60327	0.60322
1.7	-	0.600	0.60091	0.60090
1.5	0.601	0.601	0.60099	0.60099
1.3	0.603	0.603	0.60346	0.60345
1.0	0.616	0.616	0.61591	0.61591
0.8	0.636	0.636	0.63608	0.63610
0.5	0.713	0.712	0.71322	0.71101

Table 4.3 – Comparison between present calculation of $-H(\infty)$ and results of Andersson et al. [35], Ming et al. [25] and Mitschka (1965) [34].

n	$-H(\infty)$			
	Mitschka [34]	Andersson [35]	Ming [25]	Present
2.0	-	0.586	0.58765	0.58972
1.7	-	0.633	0.63662	0.63662
1.5	0.678	0.676	0.67828	0.67618
1.3	0.735	0.735	0.73591	0.73534
1.0	-	0.883	0.88230	0.88346
0.8	1.052	1.089	1.05929	1.06436
0.5	1.513	1.539	1.54389	1.54511

4.4 Numerical results with discussion

Under this heading we presented the computational results in the form of tables and graphs with their discussion. MATLAB built-in solver *bvp4c* is used to analyze the effect of variations in POWER-LAW index n, volume fraction parameter ϕ on both temperature and velocity profiles of Cu-water and Al_2O_3-water nanofluids. Additionally the results for skin friction coefficient and Nusselt number are studied. Properties of base fluid and nanoparticles are mentioned in Table 4.4.

Table 4.4 – Properties of Nanoparticles(Cu and Al_2O_3) and base fluid (water)..

Physical properties	Base fluid Water	Nanoparticles Cu	Nanoparticles Al_2O_3
$C_p(J/kgK)$	4179	385	765
$\rho(kg/m^3)$	997.1	8933	3970
$k(W/mk)$	0.613	400	40
$\sigma(\Omega.m)^{-1}$	0.05	5.96 x 10^7	10^{-12}

4.4.1 Effect of POWER-LAW index n:

In Figures 4.2 - 4.4 effect of POWER-LAW index on radial, tangential and axial velocity components are presented. Radial velocity component F initially increases with an increase in the POWER-LAW index and after reaching its maximum value it start decreasing while both tangential and axial velocity (G and H) decreases with an increase in n for both nanofluids. The temperature profile decreases when n is increased. The velocity initially increases rapidly because of the rotational effect near the boundary of disk but as the fluid particles moves aways from the boundary of disk the velocity of shear thinning fluid first starts decreasing. This behavior is then followed by Newtonian and lastly by shear thickening fluid. This behavior is noticed because of the decrease in shear stress. Moreover the increase in viscosity is also responsible for this behavior for fluids where $n < 1$. We can easily see that the peaks of the curves in Figure 4.2 are slightly affected by the variation in n while in Figure 4.3 the shear driven motion decays rapidly in tangential direction. This effect is balanced by an increase in the axial inflow $-H(0)$. Figure 4.5 results in the decrease in thickness of boundary layer as the the POWER-LAW index n increases.
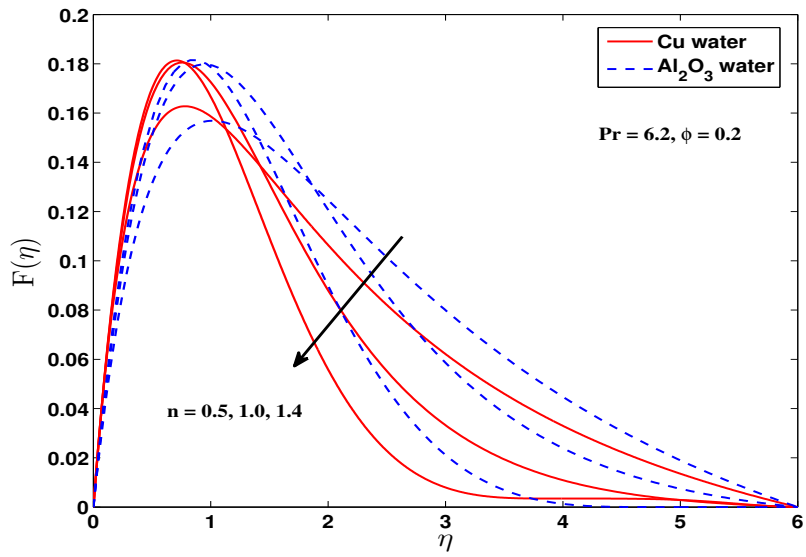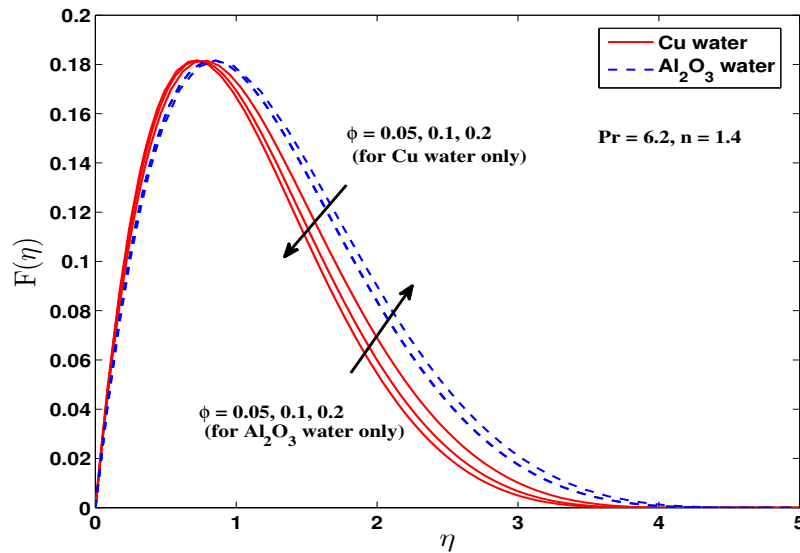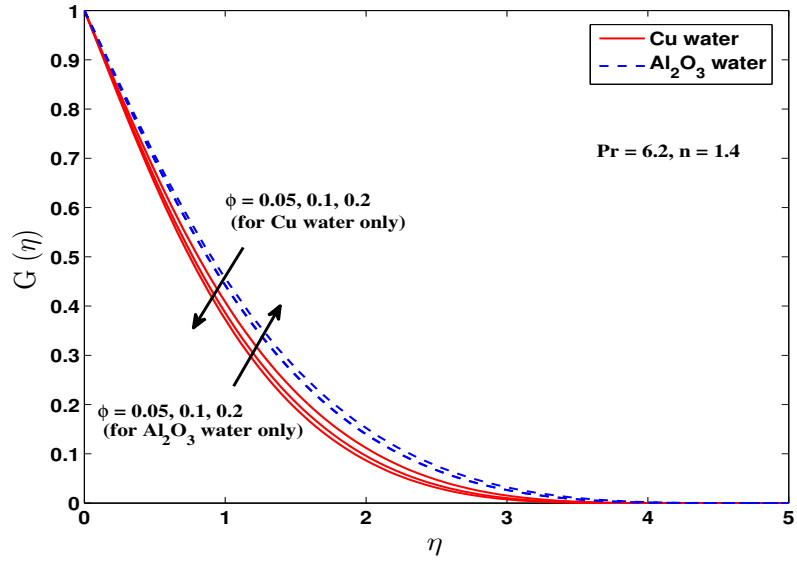
Figure 4.2 – Present lines for radial velocity for variation in n.
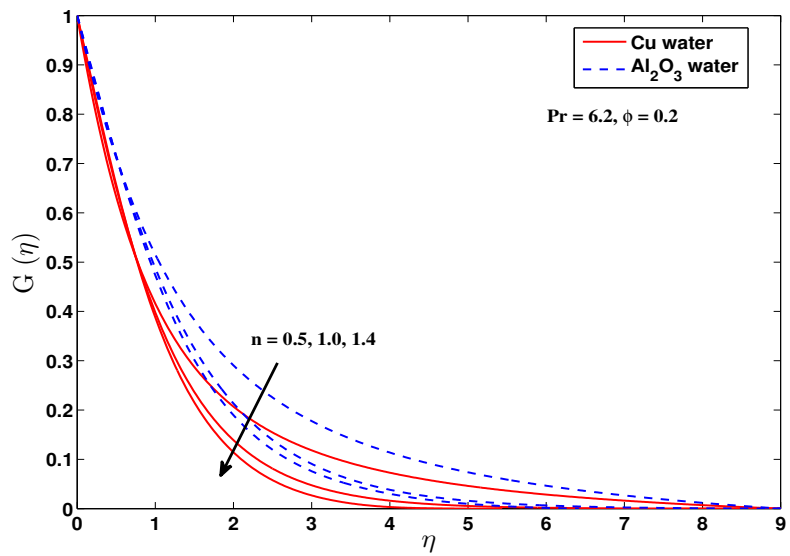
Figure 4.3 – Present lines for tangential velocity for variation in n.
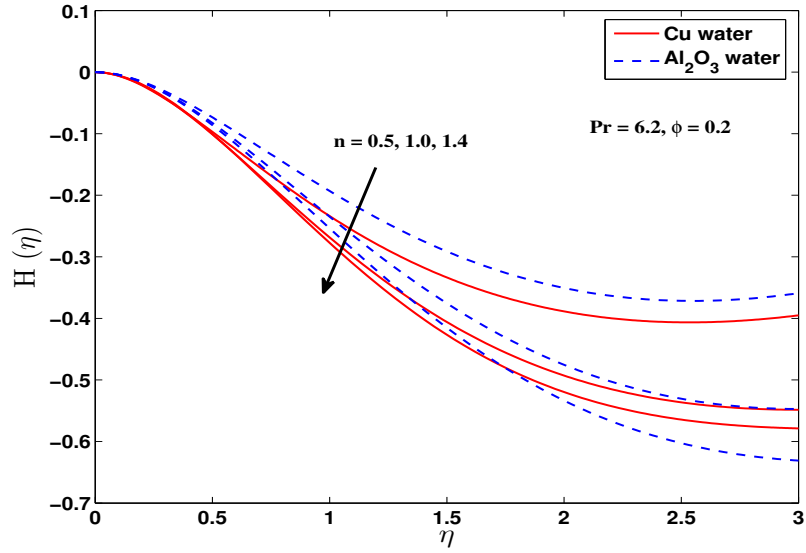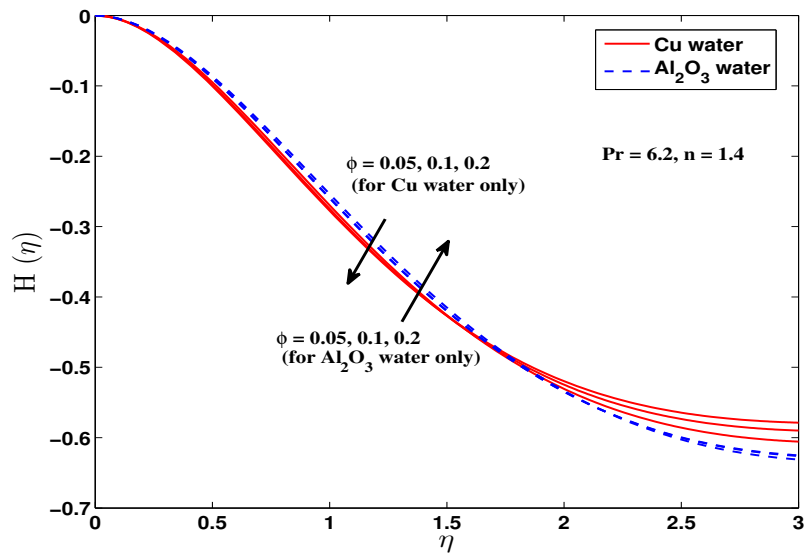
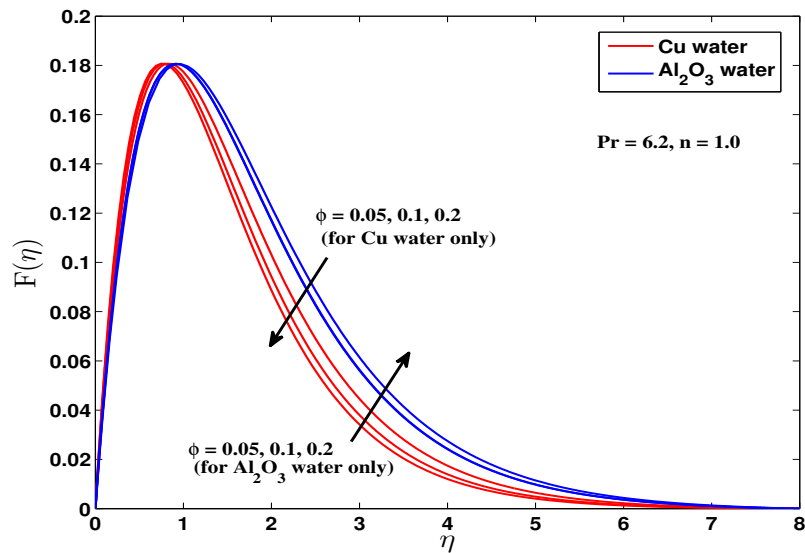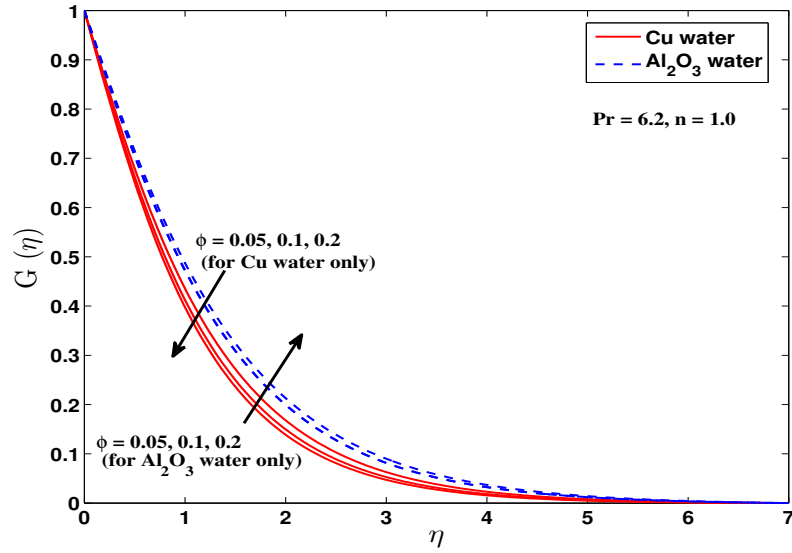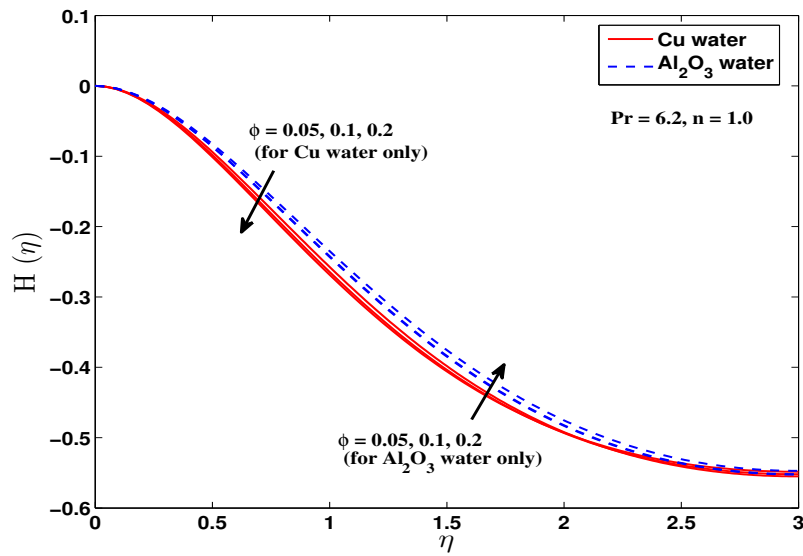Figure 4.4 – Present lines for axial velocity for variation in n.
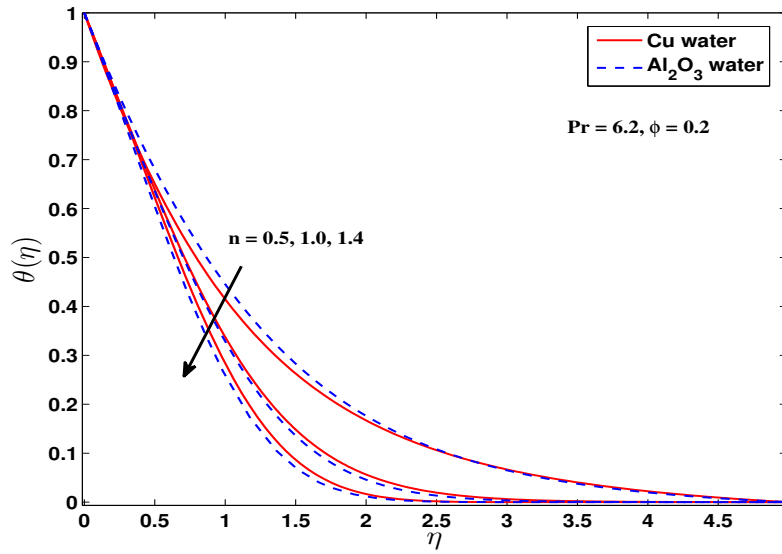
Figure 4.5 – Present lines for temperature profile for variation in n.

4.4.2 Effect of volume fraction parameter ϕ:

The consequence of varying nanoparticle volume fraction ϕ on temperature and velocity profiles can be seen in the graphs below. Figures 4.6 - 4.9 shows the behavior

of both nanofluids for shear thickening fluid with the fixed value of $n = 1.4$. In Cu-water the velocity profile of nanofluid initially increases when ϕ is increased due to the rotational effect whereas it starts decreasing after attaining maximum value at $\eta \approx 0.75$. This behavior is due to the increase in viscosity with an increase in ϕ which decreases the velocity of the nanofluid. The temperature profile also shows increasing behavior with ϕ because the increase in ϕ automatically rises the thermal conductivity which further increases the thickness of boundary layer of temperature profile. Alumina water shows the opposite behavior except for temperature profile.
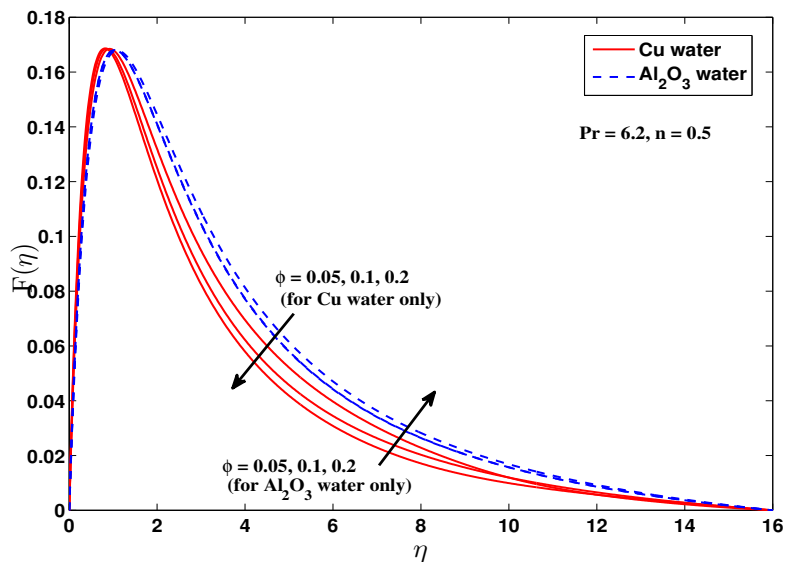

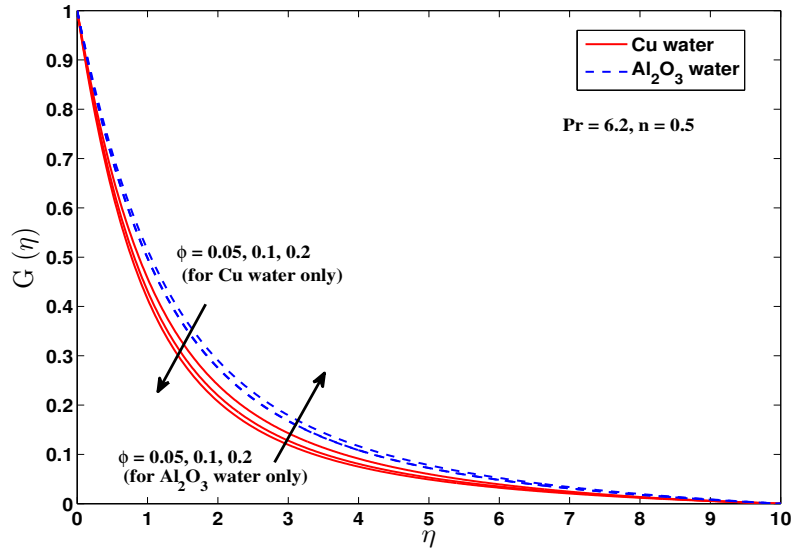Figure 4.6 – Present lines for radial velocity for variation in ϕ when $n = 1.4$.

Figure 4.7 – Present lines for tangential velocity for variation in ϕ when $n = 1.4$.

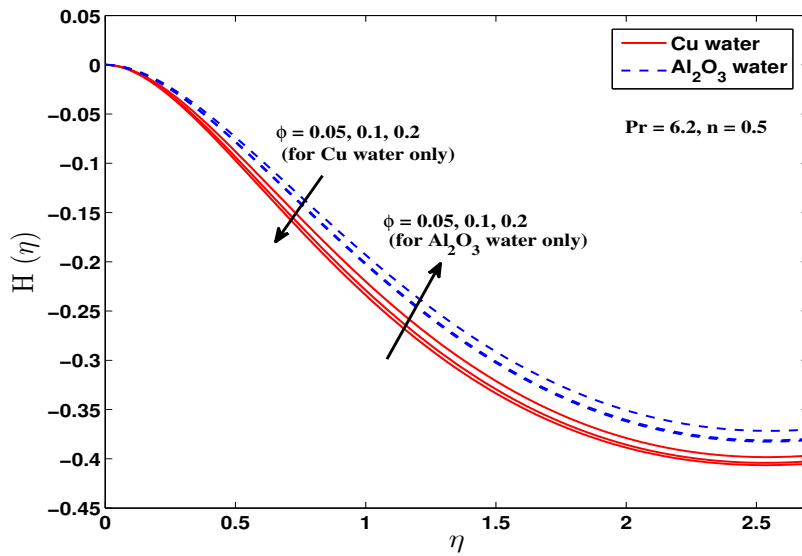Figure 4.8 – Present lines for axial velocity for variation in ϕ when $n = 1.4$.
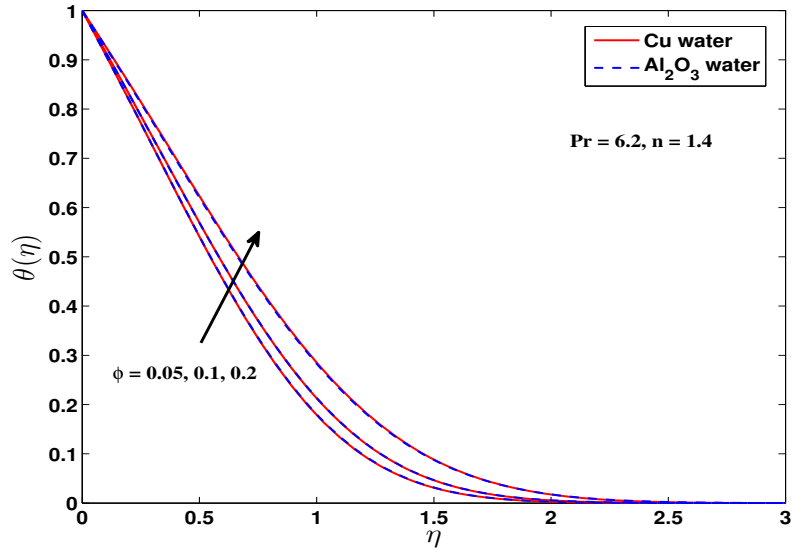
Figure 4.9 – Present lines for temperature profile for variations in ϕ when $n = 1.4$.

The Figures 4.10 - 4.13 shows the behavior of both nanofluids for Newtonian fluid with the fixed value of $n = 1.0$. The behavior of nanofluid remains the same.

Figure 4.10 – Present lines for radial velocity for variation in ϕ when $n = 1.0$.

Figure 4.11 – Present lines for tangential velocity for variation in ϕ when $n = 1.0$.

Figure 4.12 – Present lines for axial velocity for variation in ϕ when $n = 1.0$.
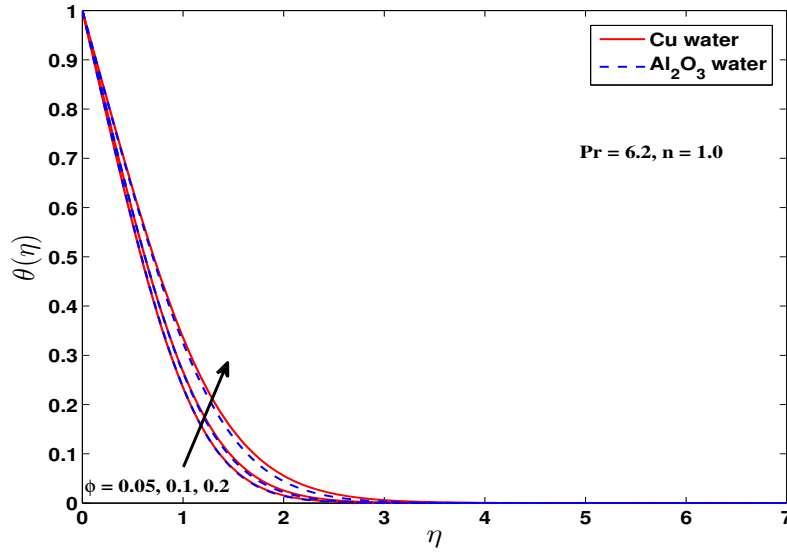
Figure 4.13 – Present lines for temperature profile for variations in ϕ when $n = 1.0$.

The Figures 4.14 - 4.17 shows the behavior of both nanofluids for shear thinning fluid when $n = 0.5$. Here the behavior of both the nanofluids become opposite except for the tempearture profile.

Figure 4.14 – Present lines for radial velocity for variation in ϕ when $n = 0.5$.

Figure 4.15 – Present lines for tangential velocity for variation in ϕ when $n = 0.5$.

Figure 4.16 – Present lines for axial velocity for variation in ϕ when $n = 0.5$.
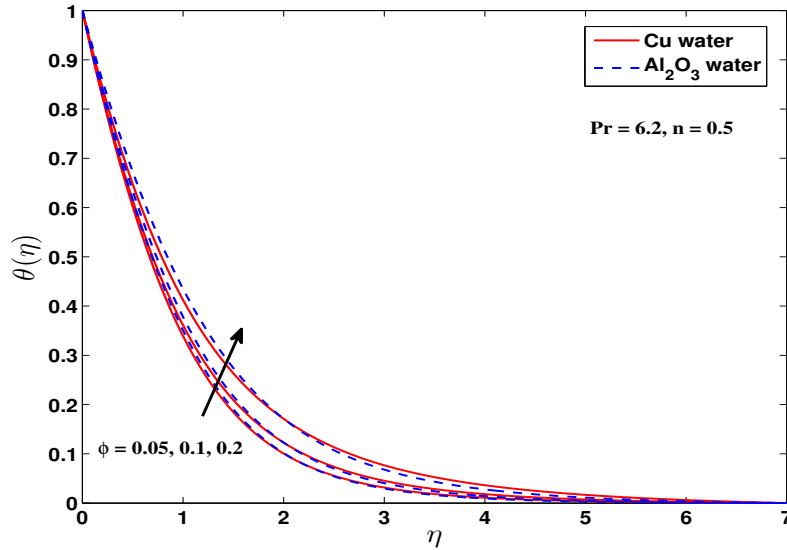
Figure 4.17 – Present lines for temperature profile for variations in ϕ when $n = 0.5$.

4.4.3 Skin friction Coefficient:

Table 4.5 exhibit the impact of parameters n and ϕ on skin friction coefficient at the disk. It is observed that at the disk skin friction coefficient increases for decreasing values of POWER-LAW index n which means that highest value of skin friction coefficient is achieved by shear thinning fluids while it increases as values of ϕ gets higher. The decrease in POWER-LAW index n shows that the velocity of the nanofluid is also decreasing which means that the magnitude of resistance shown toward the nanofluid is increasing which results in the increase of skin friction coefficient. The decrease in skin friction coefficient values results in the thickening of boundary layer of velocity profile. On the other hand free stream velocity is observed at the surface. This is evident by the increase in skin friction coefficient the rise in skin friction coefficient values corresponds to fluid velocity at the disk approaching to free stream velocity. Whereas increasing values of ϕ causes increase in skin friction coefficient.

Table 4.5 – Values of skin friction coefficient for the variation of parameters for fixed Pr = 6.2.

n	ϕ	$C_f Re_r^{1/n+1}$ Cu - water	$C_f Re_r^{1/n+1}$ $Al_2O_3 - water$
1.4	0.2	1.6035	1.2265
1.0		1.6844	1.3310
0.5		1.8163	1.5472
1.4	0.05	0.9337	0.8366
	0.1	1.1445	0.9555
	0.2	1.6035	1.2265
1.0	0.05	0.9940	0.9026
	0.1	1.2085	1.0311
	0.2	1.6844	1.3310
0.5	0.05	1.1052	1.0351
	0.1	1.3184	1.1833
	0.2	1.8163	1.5472

4.4.4 Nusselt number:

The Table 4.6 shows impact of parameters n and ϕ on Nusselt number at the disk. It is found that for Cu-water at the disk Nusselt number increases for decreasing values of POWER-LAW index n. This proves that the rate of decrease in temperature is minimum for fluids having $n > 1$. Also the increasing values of Nusselt number directly corresponds to rise in rate of heat dissipation. This also results in the thinning of thermal boundary layer. Whereas increasing values of ϕ causes increase in Nusselt number.

Table 4.6 – Values of Nusselt Number for the variation of parameters for fixed Pr = 6.2.

n	ϕ	$-Nu_r Re_r^{-1/n+1}$ Cu - water	$-Nu_r Re_r^{-1/n+1}$ $Al_2O_3 - water$
1.4	0.2	-1.2496	-1.1940
1.0		-1.2625	-1.1276
0.5		-1.4568	-1.1165
1.4	0.05	-1.0262	-1.0105
	0.1	-1.0992	-1.0708
	0.2	-1.2496	-1.1940
1.0	0.05	-0.9990	-0.9590
	0.1	-1.0894	-1.0170
	0.2	-1.2625	-1.1276
0.5	0.05	-1.0139	-0.9192
	0.1	-1.1685	-0.9896
	0.2	-1.4508	-1.1165

Chapter 5

NUMERICAL RESULTS FOR MHD SLIP FLOW OF POWER-LAW NANOFLUID OVER AN INFINITE ROTATING DISK WITH HEAT TRANSFER

This chapter covers the study of heat transfer and MHD slip flow characteristics of POWER-LAW nanofluid over a rotating disk. Slip conditions are assumed at the boundary and variable viscosity as well as thermal conductivity is again taken into account.

5.1 Mathematical model

Here we extended the mathematical model presented in the last chapter and include a uniform magnetic field **B** over an infinite disk. The disk is rotating with an angular velocity having constant value Ω. Constitutive equations of conservation mass, z-momentum and thermal energy remains same as (4.1.2), (4.1.5) and (4.1.6) while the r-momentum and θ momentum equations under boundary layer approximation takes the form

$$\rho_{nf}\left(v_1\frac{\partial v_1}{\partial r} + v_3\frac{\partial v_1}{\partial z} - \frac{v_2{}^2}{r}\right) = \frac{\partial}{\partial z}\left(\mu_{nf}\frac{\partial v_1}{\partial z}\right) - \sigma_{nf}v_1 B_0{}^2, \qquad (5.1.1)$$

$$\rho_{nf}\left(v_1\frac{\partial v_2}{\partial r} + v_3\frac{\partial v_2}{\partial z} + \frac{v_1 v_2}{r}\right) = \frac{\partial}{\partial z}\left(\mu_{nf}\frac{\partial v_2}{\partial z}\right) - \sigma_{nf}v_2 B_0{}^2, \qquad (5.1.2)$$

The viscosity function is given in equation (4.1.7) and the variable thermal conductivity of the nanofluid is given in equation (4.1.9) of the previous section. The slip boundary conditions are

$$v_1 = L_1\left[\frac{\partial v_1}{\partial z}\right]^{\frac{n-1}{2}}, v_2 = \Omega r + L_2\left[\frac{\partial v_1}{\partial z}\right]^{\frac{n-1}{2}}, v_3 = 0,\ T = T_w\ \ \text{at}\ \ z = 0, \qquad (5.1.3)$$

$$v_1 = 0 = v_2,\ T \to T_\infty\ \text{as}\ z \to \infty, \qquad (5.1.4)$$

while for the limiting case of large z, axial velocity (v_3) approach some unknown constant. Here L_1 and L_2 are the velocity slip parameters.

5.2 Similarity transformation

Now we transform the above boundary layer equations (5.1.1)-(5.1.2) along with the boundary conditions (5.1.3) and (5.1.4) into the following ODEs using variables η, u, v, w and θ defined in equations (4.2.1)-(4.2.3)

$$\mathbf{U}\left[F^2 - G^2 + \left(H + \frac{1-n}{1+n}\eta F\right)F'\right] = \left[\left(F'^2 + G'^2\right)^{(n-1)/2}F'\right]' - m\frac{\sigma_{nf}}{\sigma_f}F, \ (5.2.1)$$

$$\mathbf{U}\left[2FG + \left(H + \frac{1-n}{1+n}\eta F\right)G'\right] = \left[\left(F'^2 + G'^2\right)^{(n-1)/2} G'\right]' - m\frac{\sigma_{nf}}{\sigma_f}G, \quad (5.2.2)$$

where m represents magnetic parameter which is basically the Hartman number and has the relation

$$m = \frac{\sigma_f B_0^2}{\rho_f \Omega}. \quad (5.2.3)$$

The boundary conditions (5.1.3)-(5.1.4) are likewise transformed into

$$F = A_1(F')^{\frac{n-1}{2}}, \ G = 1 + A_2(F')^{\frac{n-1}{2}}, \ H = 0, \ \theta = 1 \ \text{ at } \ \eta = 0, \quad (5.2.4)$$

$$F = 0, \ G = 0, \ \theta = 0 \text{ as } \eta \to \infty. \quad (5.2.5)$$

Again the important quantities of interest are Nusselt number and skin friction coefficient which are given in equation (4.2.9) and equation (4.2.10).

5.3 Numerical method for solution

Now we transform the above BVP (5.2.1)-(5.2.2) along with (4.2.4) and (4.2.7) to initial value problem (IVP) of first order having dependent variables y_1, y_2, y_3, y_4, y_5, y_6 and y_7 such that $y_1 = F$, $y_2 = F'$, $y_3 = G$, $y_4 = G'$, $y_5 = H$, $y_6 = \theta$ and $y_7 = \theta'$. Denote

$$J = \left(y_2^2 + y_4^2\right)^{\frac{1-n}{2}}, \quad (5.3.1)$$

$$K = \left(y_2^2 + y_4^2\right)^{-1}, \quad (5.3.2)$$

$$L = y_5 + \frac{1-n}{1+n}\eta y_1, \quad (5.3.3)$$

$$M = y_1^2 - y_3^2 + \left(y_5 + \frac{1-n}{1+n}\eta y_1\right)y_2, \quad (5.3.4)$$

$$N = 2y_1 y_3 + \left(y_5 + \frac{1-n}{1+n}\eta y_1\right)y_4. \quad (5.3.5)$$

Therefore, we can write the coupled seven equations of first order as

$$y_1' = y_2, \quad (5.3.6)$$

$$y_2' = \mathbf{U}\frac{1}{n}J\left[M\left(1+(n-1)Ky_4^2\right)-(n-1)KNy_2y_4\right]+\left(\frac{mJy_1}{n}\frac{\sigma_{nf}}{\sigma_f}\right) \tag{5.3.7}$$

$$+m\frac{\sigma_{nf}}{\sigma_f}JK[y_2y_4{}^2-y_2y_3y_4]+\frac{m\sigma_{nf}JK}{n\sigma_f}[y_2y_3y_4-y_2y_4{}^2],$$

$$y_3' = y_4, \tag{5.3.8}$$

$$y_4' = \mathbf{U}\frac{1}{n}J\left[N\left(1+(n-1)Ky_2^2\right)-(n-1)KMy_2y_4\right]+\left(\frac{mJy_3}{n}\frac{\sigma_{nf}}{\sigma_f}\right) \tag{5.3.9}$$

$$+m\frac{\sigma_{nf}}{\sigma_f}JK[y_2{}^2y_3-y_1y_2y_4]+\frac{m\sigma_{nf}JK}{n\sigma_f}[y_1y_2y_4-y_2{}^2y_3],$$

$$y_5' = -2y_1-\frac{1-n}{1+n}\eta y_2, \tag{5.3.10}$$

$$y_6' = y_7, \tag{5.3.11}$$

$$y_7' = Jy_7\left[L\left(Pr\mathbf{Q}-\frac{(n-1)}{n}\mathbf{U}\right)-\left(\frac{n-1}{n}\right)\mathbf{U}K\left(2y_1y_3y_4+y_1{}^2y_2-y_2y_3{}^2\right)\right] \tag{5.3.12}$$

$$-Jy_7\left(\frac{n-1}{n}\right)Km\left(\frac{\sigma_{nf}}{\sigma_f}\right)(y_1y_2+y_3y_4),$$

where $\mathbf{Q}$ and $\mathbf{U}$ are given in equations (4.3.13) and (4.3.14).

5.3.1   Verification of numerical results

We compared our results with Andersson et al. [43] by taking several values of magnetic field parameter m and by assuming $\phi = 0$ and $Pr = 6.2$, for the particular case of Newtonian fluid ($n = 1$). The comparison is given in Table 5.1 which shows that the present results are in a good agreement with that of Andersson et al. [43].

Table 5.1 – Comparison between present calculation of $F'(0)$, $-G'(0)$, $-H(\infty)$ and results of Andersson et al. [43].

	$F'(0)$		$-G'(0)$		$-H(\infty)$	
m	Andersson [43]	Present	Andersson [43]	Present	Andersson [43]	Present
0	0.5101	0.51022	0.6101	0.61591	0.8827	0.88320
0.5	0.3851	0.38513	0.8487	0.84872	0.4589	0.45879
1.0	0.3093	0.30925	1.0691	1.06905	0.2533	0.25330
2.0	0.2306	0.23055	1.4421	1.44209	0.1086	0.10858
4.0	0.1654	0.16570	2.0103	2.01026	0.0408	0.04077

5.4 Numerical results with discussion

To analyze the numerical results presented in the form of tables and graphs we used the MATLAB built-in solver *bvp4c*. We studied the behavior of velocity and temperature profiles of Cu-water and Al_2O_3-water nanofluids along with the behavior of skin friction coefficient and Nusselt number with variations in POWER-LAW index n, volume fraction parameter ϕ, magnetic parameter m and velocity slip parameters A_1, A_2. We can see the physical properties of the base fluid and nanoparticles from Table 4.4.

5.4.1 Effect of POWER-LAW index n and ϕ:

The effect of POWER-LAW index n and nanoparticle concentration ϕ on both temperature and velocity profile remains the same as discussed in sections 4.4.1 and 4.4.2 of the previous chapter.

5.4.2 Effect of magnetic parameter m:

The behavior of temperature and velocity profile for variation in magnetic parameter m can be seen in the graphs given below. The Figures 5.1 - 5.4 shows the behavior of both nanofluids for shear thickening fluid ($n = 1.4$). Similarly the Figures 5.5 - 5.8 shows the behavior of Newtonian fluid ($n = 1.0$) and Figures 5.9 - 5.12 represents shear thinning fluid ($n = 0.5$).

Initially the velocity of nanofluid increases because of the strong rotational effect near the disk then after reaching its maximum value it starts decreasing with increase in m. This trend is because of the production of Lorentz force due to the applied magnetic field which shows resistance towards the motion of nanofluid. This also results as increase in thinning of boundary layer. The increase in axial velocity is basically to compensate the outward radial flow F.

The temperature of nanofluid rises as magnitude of magnetic parameter m increases because as m increase the density of the nanofluid decrease.
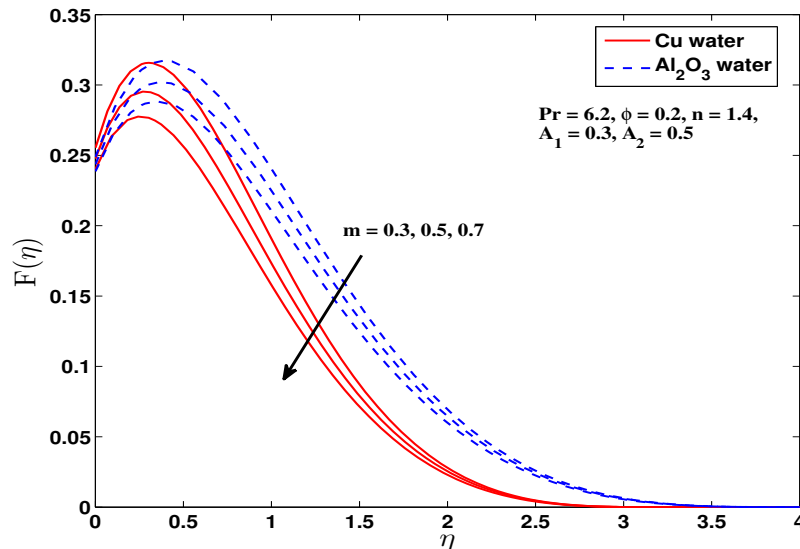
Figure 5.1 – Present lines for radial velocity for variation in m when $n = 1.4$.
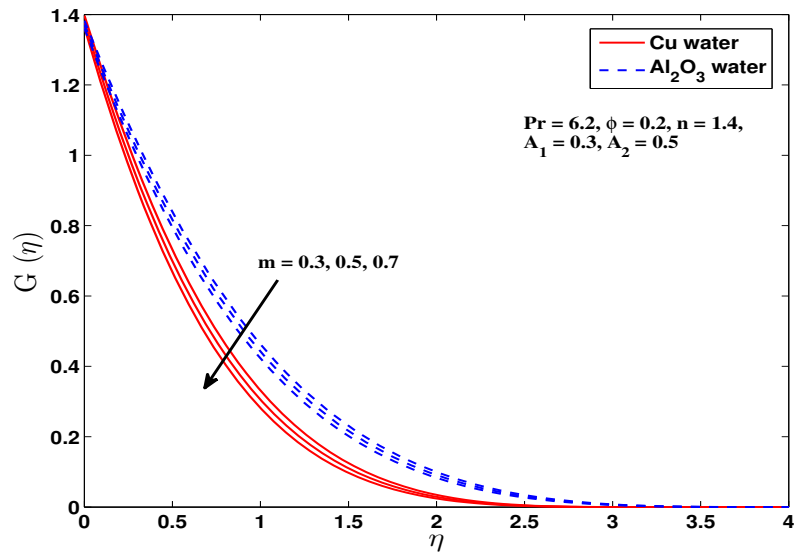
Figure 5.2 – Present lines for tangential velocity for variation in m when $n = 1.4$.
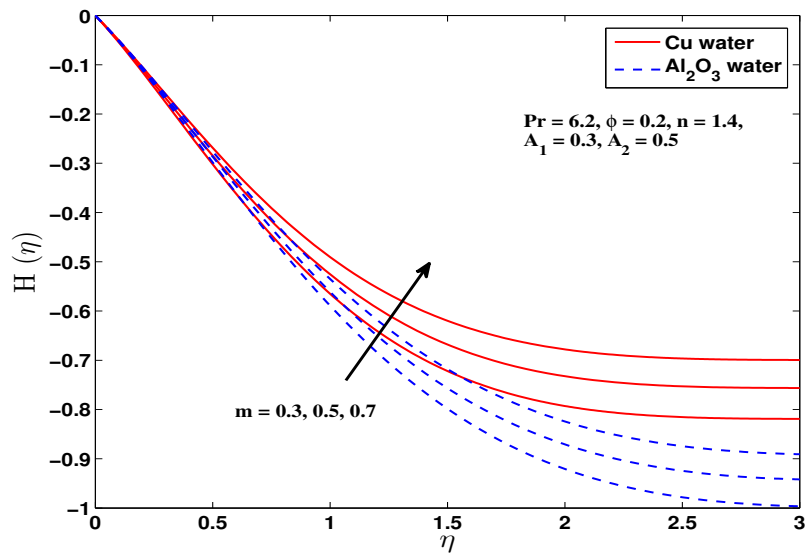
Figure 5.3 – Present lines for axial velocity for variation in m when $n = 1.4$.
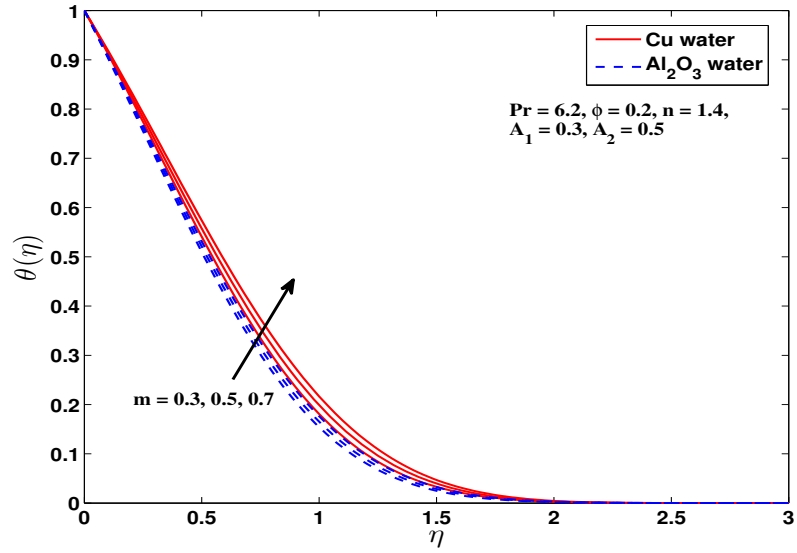
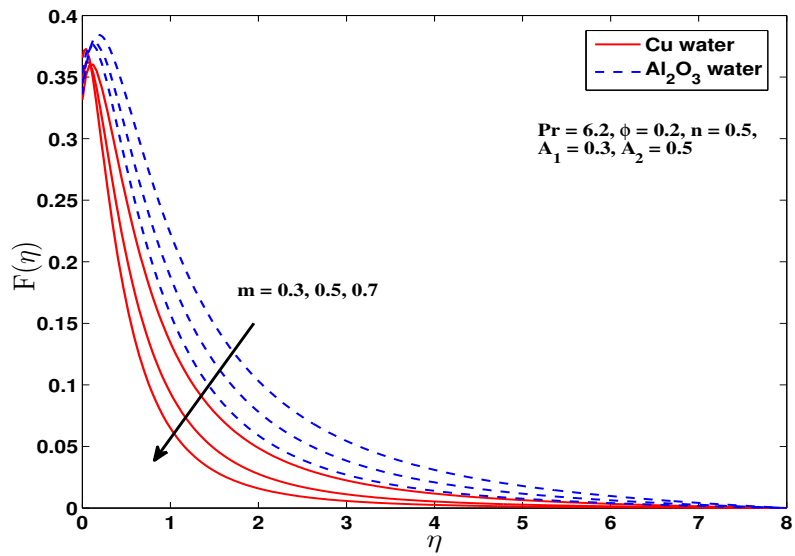Figure 5.4 – Present lines for temperature profile for variation in m when $n = 1.4$.
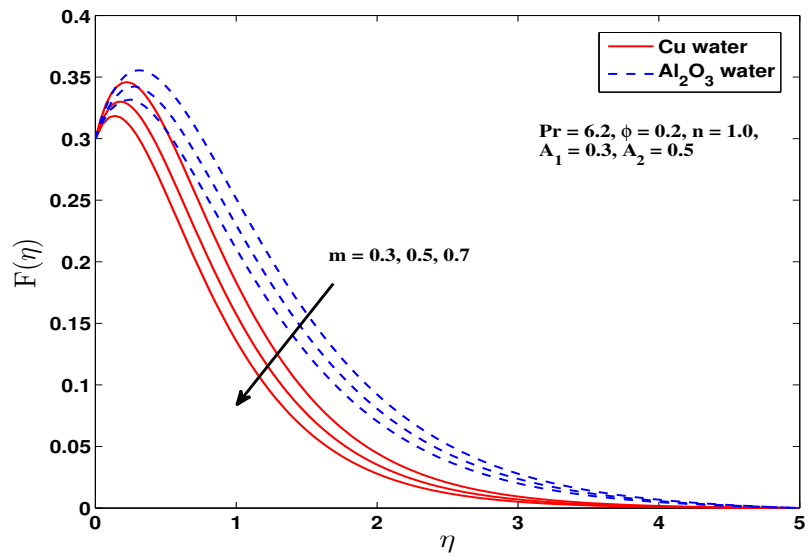
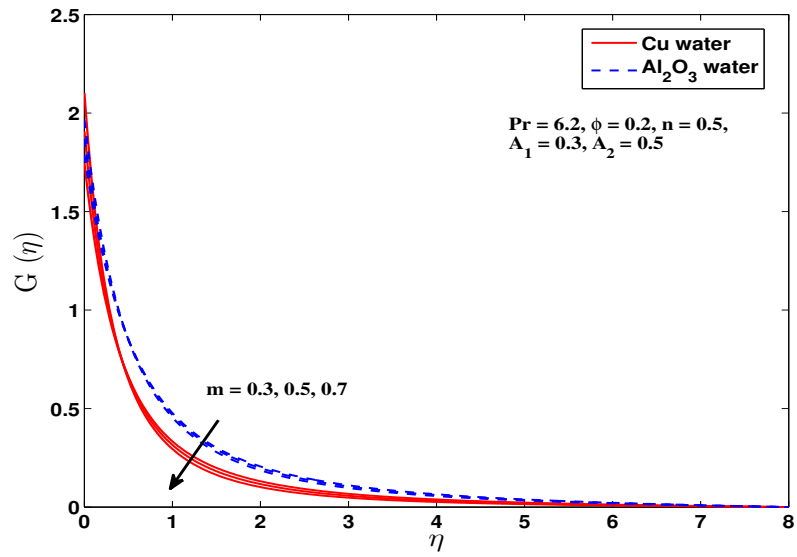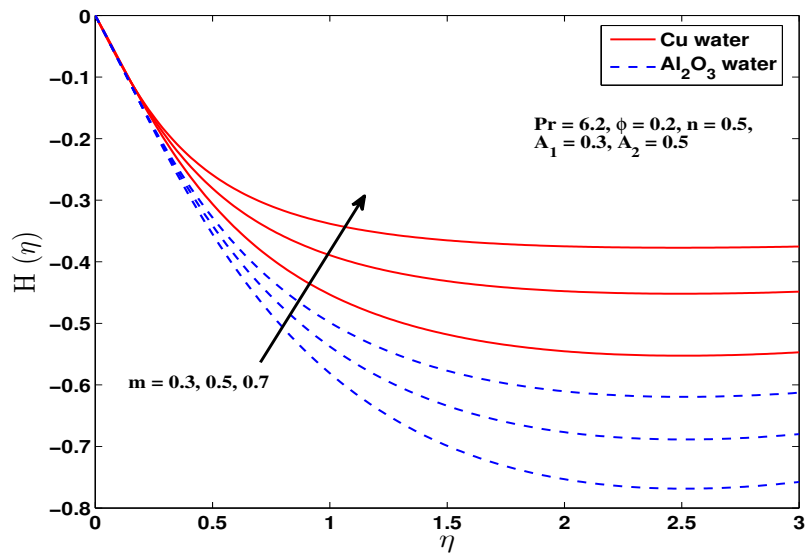Figure 5.5 – Present lines for radial velocity for variation in m when $n = 1.0$.
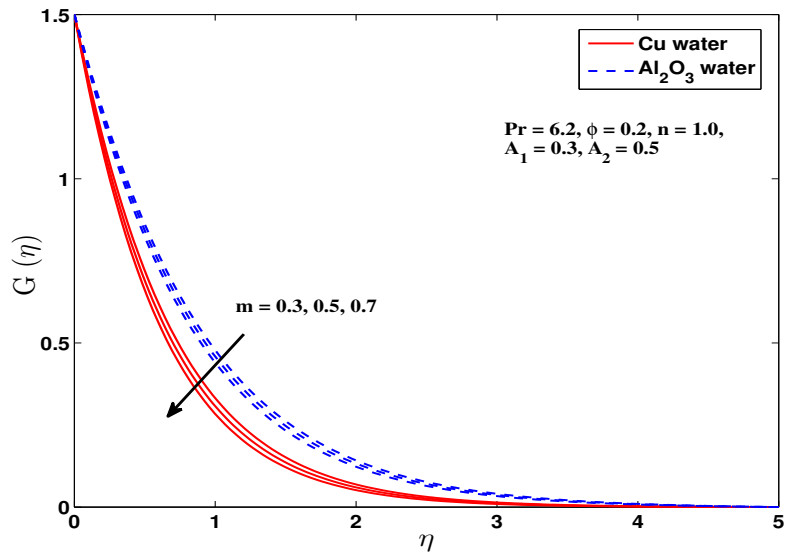
Figure 5.6 – Present lines for tangential velocity for variation in m when $n = 1.0$.
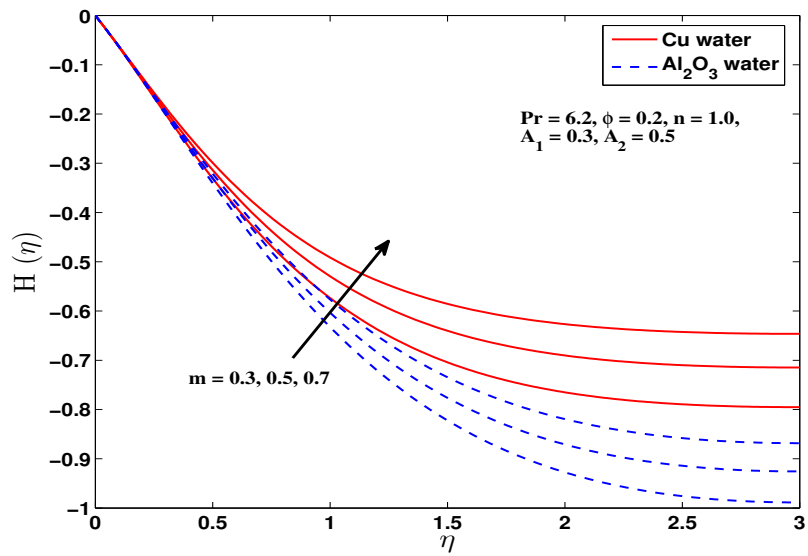
Figure 5.7 – Present lines for axial velocity for variation in m when $n = 1.0$.

58
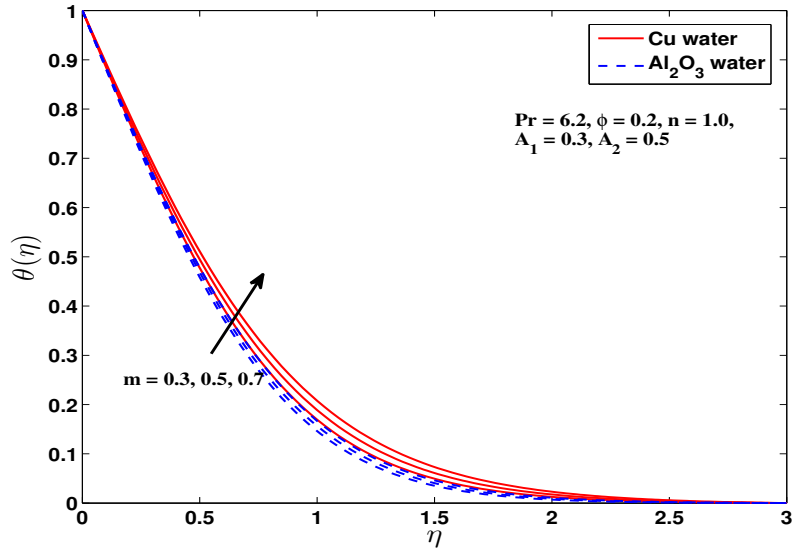
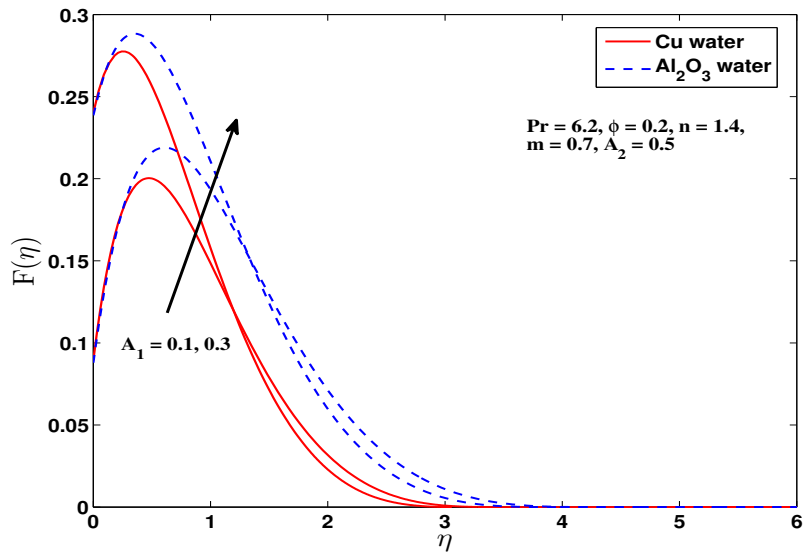Figure 5.8 – Present lines for temperature profile for variation in m when $n = 1.0$.

Figure 5.9 – Present lines for radial velocity for variation in m when $n = 0.5$.

Figure 5.10 – Present lines for tangential velocity for variation in m when $n = 0.5$.

Figure 5.11 – Present lines for axial velocity for variation in m when $n = 0.5$.
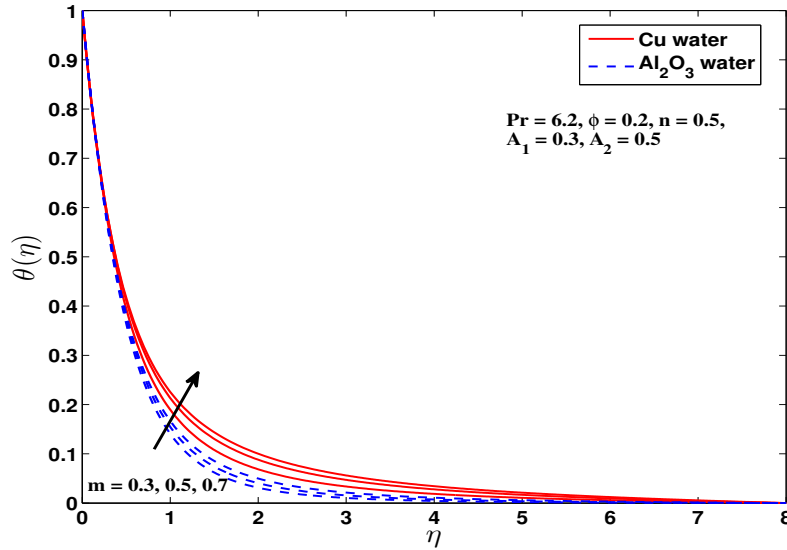
Figure 5.12 – Present lines for temperature profile for variation in m when $n = 0.5$.

5.4.3 Effect of velocity slip parameter A_1:

The effect of using different values of velocity slip parameter A_1 on temperature and velocity profiles can be seen in the graphs given below. Figures 5.13 - 5.16 shows the behavior of both nanofluids for shear thickening fluid ($n = 1.4$). Similarly the Figures 5.17 - 5.20 shows the behavior of Newtonian fluid ($n = 1.0$) and Figures 5.21 - 5.24 represents shear thinning fluid ($n = 0.5$).

A rise in value of velocity slip parameter allow a great amount of fluid to slip past the disk which proceed to an increase the flow of nanofluid through boundary layer. Thus the thickness of velocity boundary layer decrease.

Similarly increase in velocity slip parameter A_1 causes reduction in the transport of momentum in radial direction.

Also increase in A_1 at the boundary increase the rate of heat transfer. With an increase in A_1 the temperature profile become thinner.

61

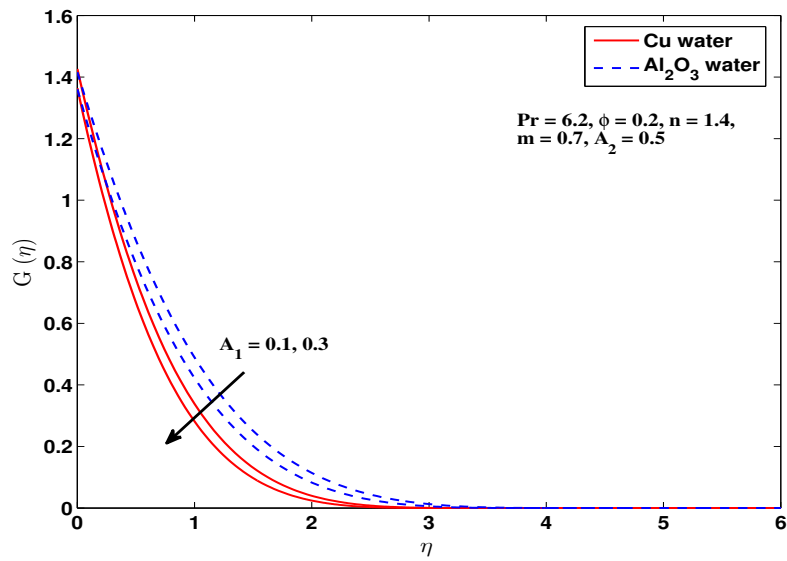Figure 5.13 – Present lines for radial velocity for variation in A_1 when $n = 1.4$.

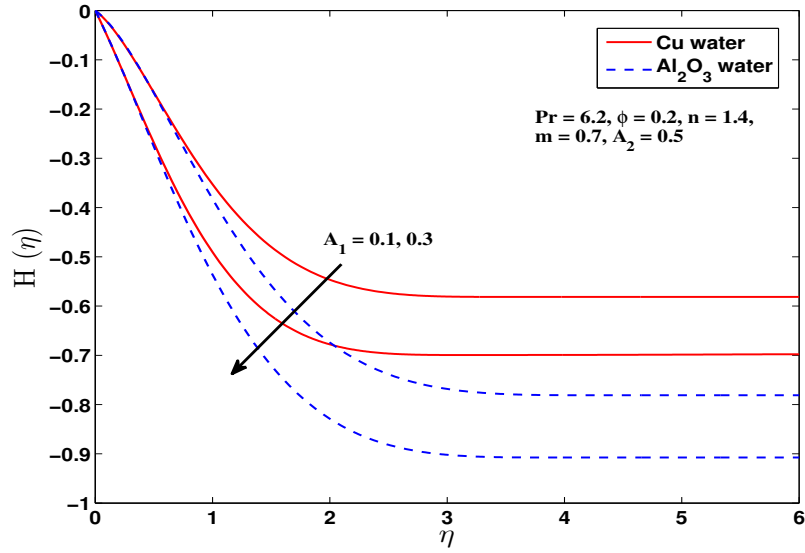Figure 5.14 – Present lines for tangential velocity for variation in A_1 when $n = 1.4$.

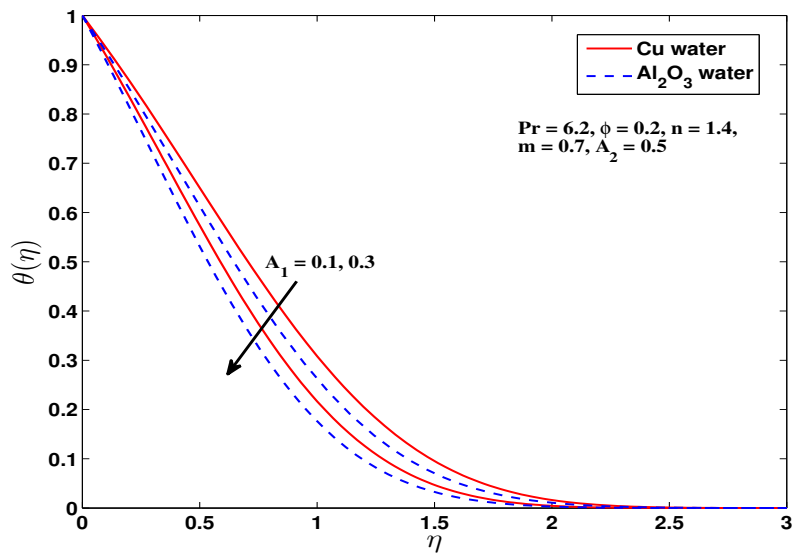Figure 5.15 – Present lines for axial velocity for variation in A_1 when $n = 1.4$.

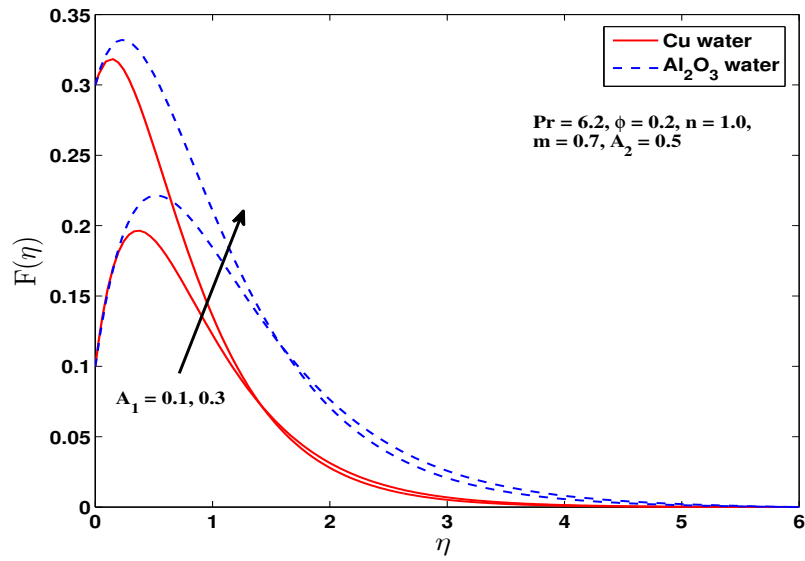Figure 5.16 – Present lines for temperature profile for variation in A_1 when $n = 1.4$.

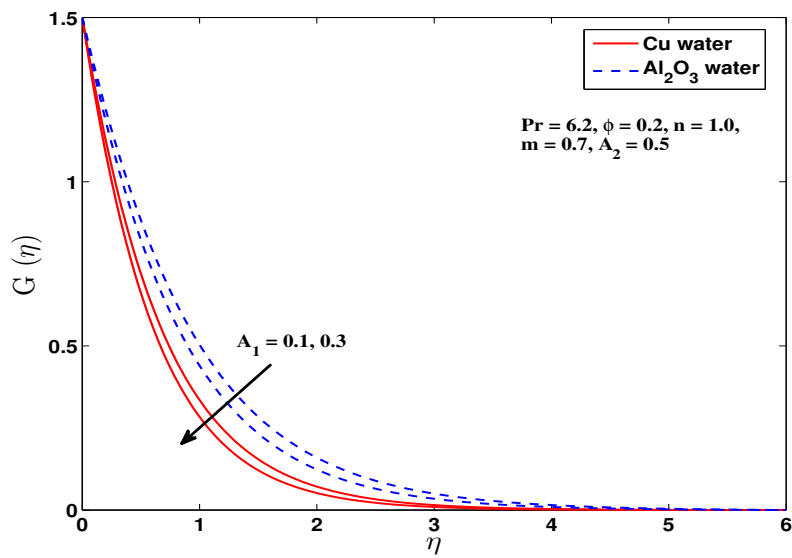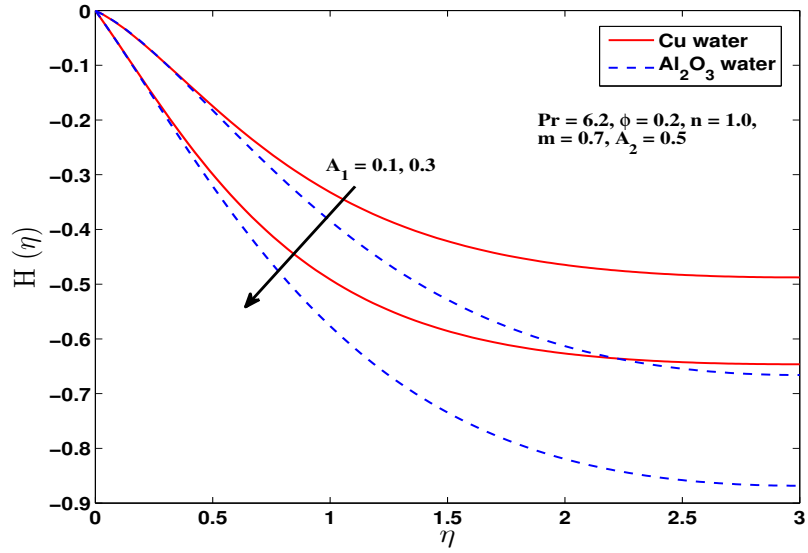Figure 5.17 – Present lines for radial velocity for variation in A_1 when $n = 1.0$.

Figure 5.18 – Present lines for tangential velocity for variation in A_1 when $n = 1.0$.

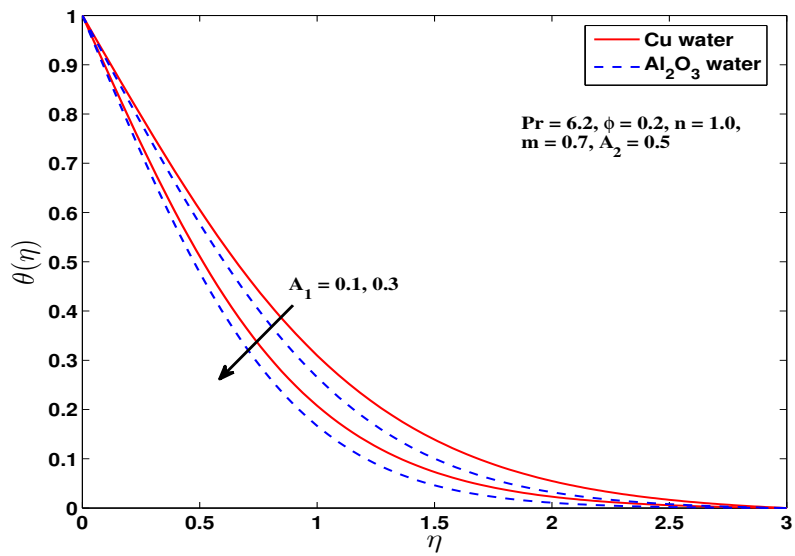Figure 5.19 – Present lines for axial velocity for variation in A_1 when $n = 1.0$.

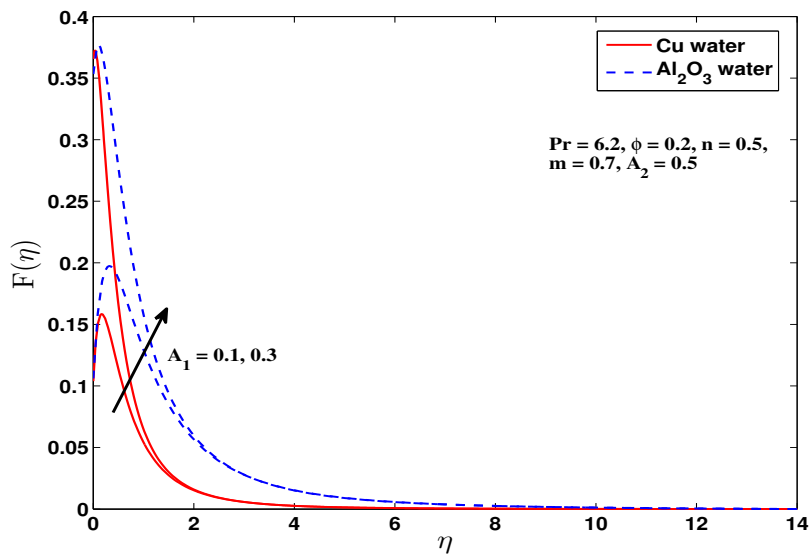Figure 5.20 – Present lines for temperature profile for variation in A_1 when $n = 1.0$.

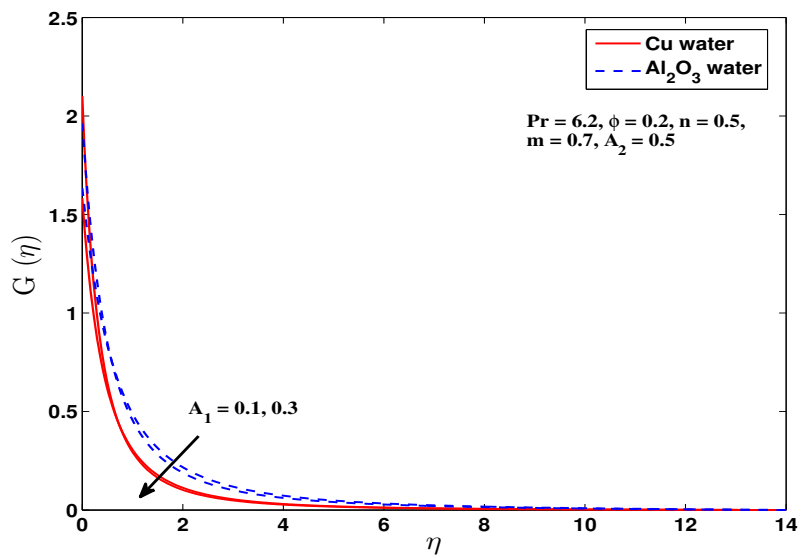Figure 5.21 – Present lines for radial velocity for variation in A_1 when $n = 0.5$.

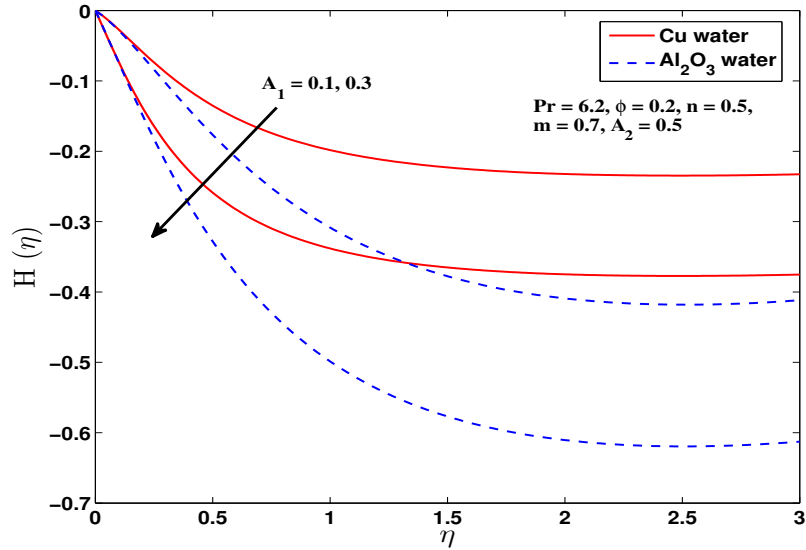Figure 5.22 – Present lines for tangential velocity for variation in A_1 when $n = 0.5$.

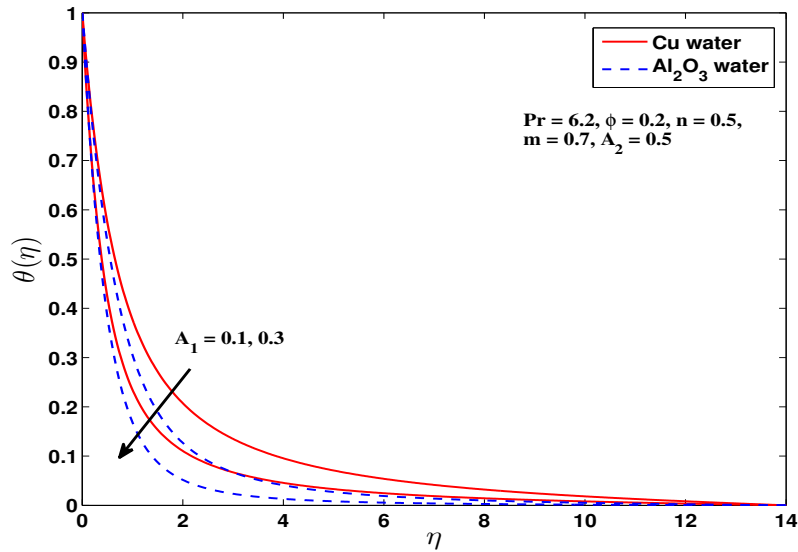Figure 5.23 – Present lines for axial velocity for variation in A_1 when $n = 0.5$.

Figure 5.24 – Present lines for temperature profile for variation in A_1 when $n = 0.5$.

5.4.4 Effect of velocity slip parameter A_2:

The effect of having different values of velocity slip parameter A_2 on both velocity and temperature profile can be seen in the graphs given below. Figures 5.25 - 5.28

shows the behavior of both nanofluids for shear thickening fluid ($n = 1.4$). Similarly the Figures 5.29 - 5.32 shows the behavior of Newtonian fluid ($n = 1.0$) and Figures 5.33 - 5.36 represents shear thinning fluid ($n = 0.5$).

For shear thickening and Newtonian fluid the flow behavior remains roughly the same as discussed for the previous case of variation in A_1. While for shear thinning fluid our graphs (5.33 - 5.31) are showing quite opposite behavior.

Figure 5.25 – Present lines for radial velocity for variation in A_2 when $n = 1.4$.

Figure 5.26 – Present lines for tangential velocity for variation in A_2 when $n = 1.4$.

Figure 5.27 – Present lines for axial velocity for variation in A_2 when $n = 1.4$.

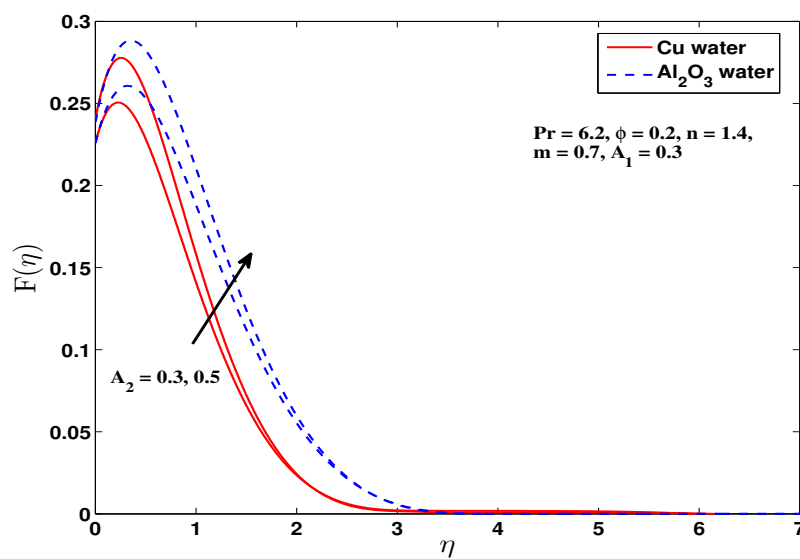Figure 5.28 – Present lines for temperature profile for variation in A_2 when $n = 1.4$.

Figure 5.29 – Present lines for radial velocity for variation in A_2 when $n = 1.0$.

Figure 5.30 – Present lines for tangential velocity for variation in A_2 when $n = 1.0$.
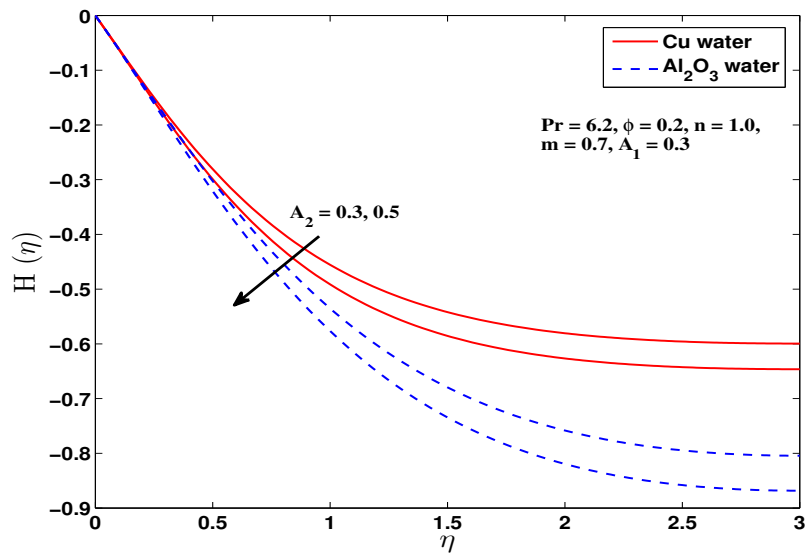
Figure 5.31 – Present lines for axial velocity for variation in A_2 when $n = 1.0$.
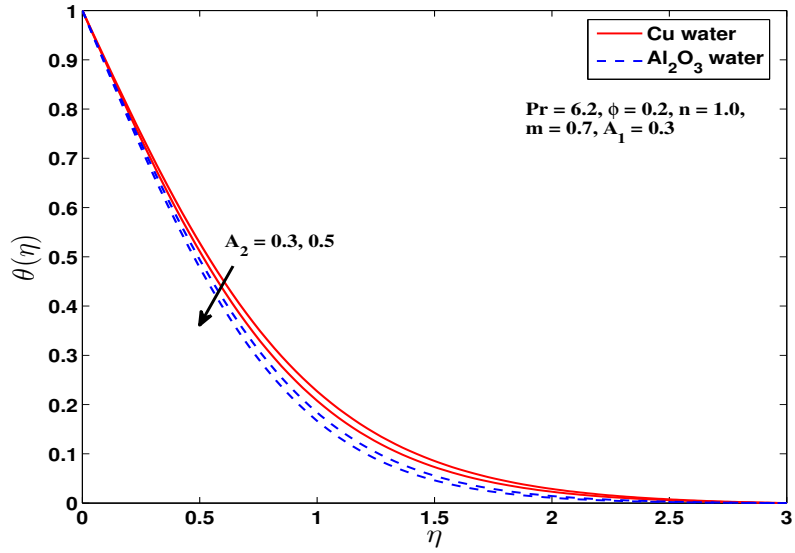
Figure 5.32 – Present lines for temperature profile for variation in A_2 when $n = 1.0$.
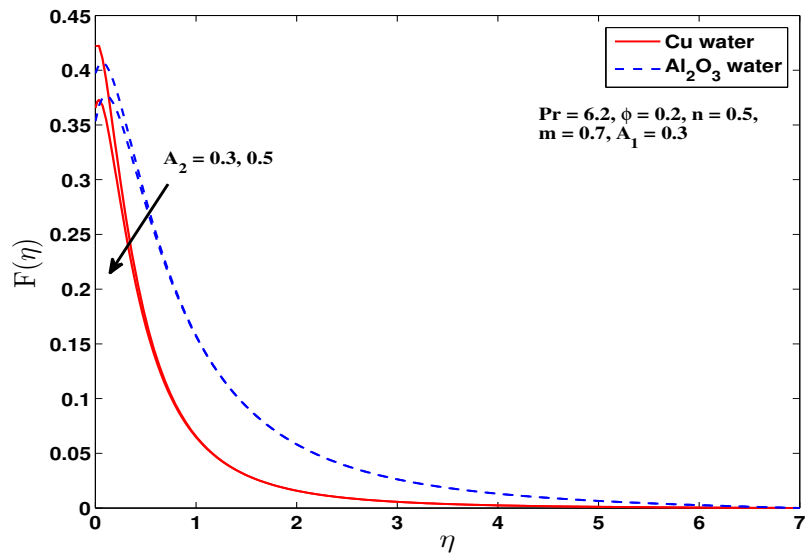
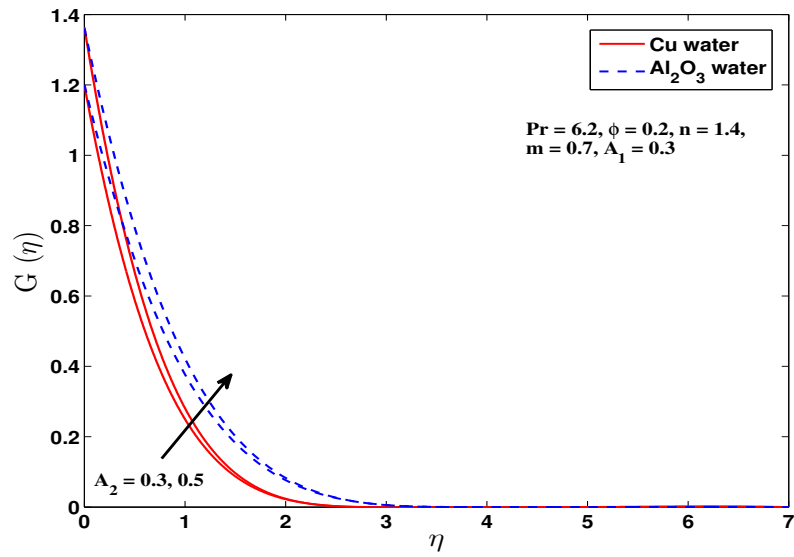Figure 5.33 – Present lines for radial velocity for variation in A_2 when $n = 0.5$.

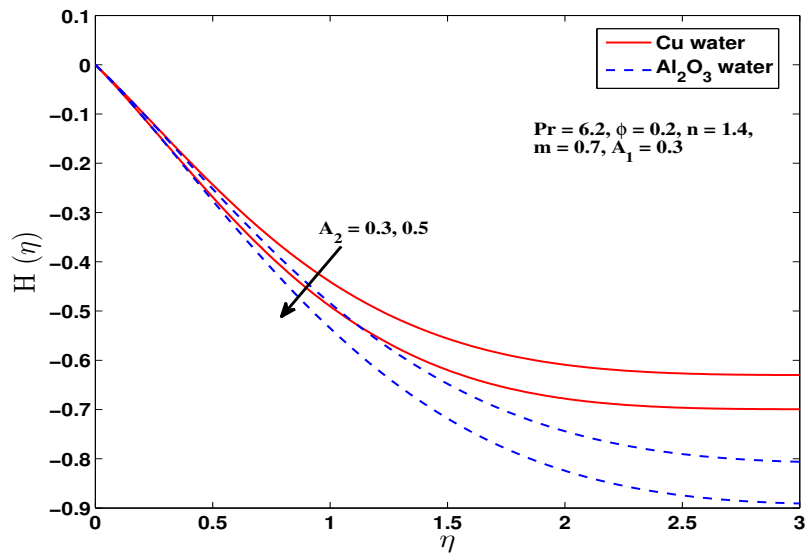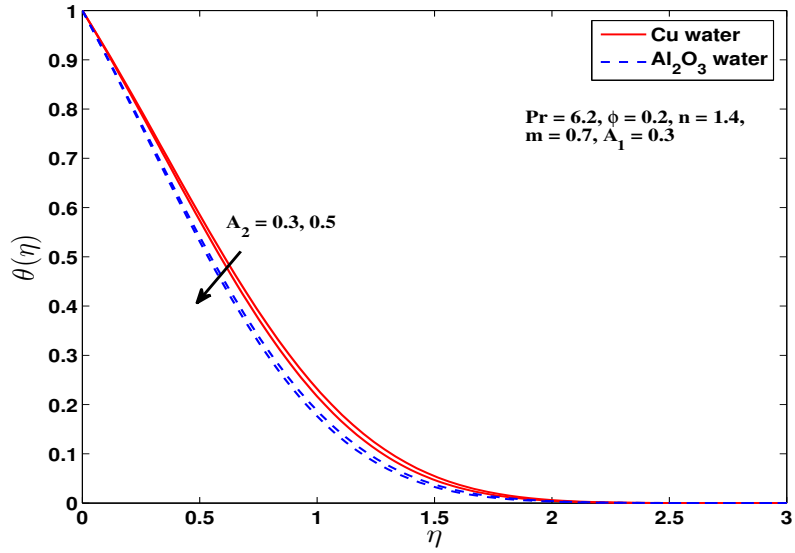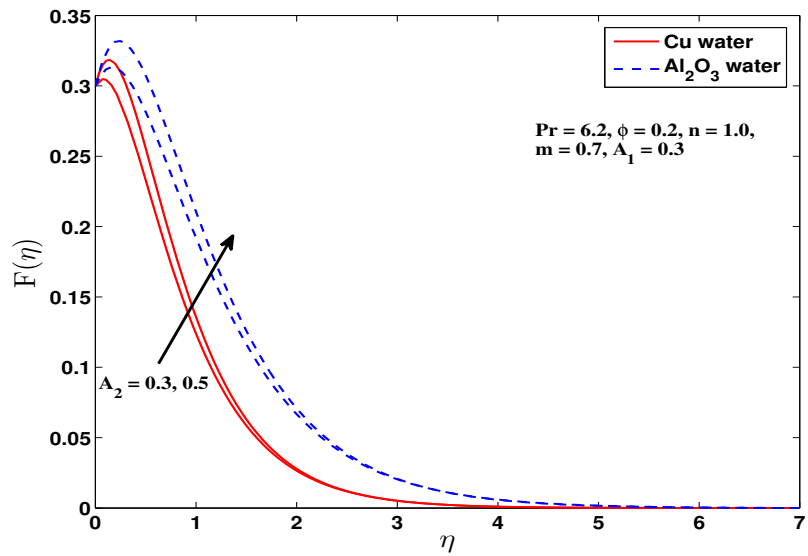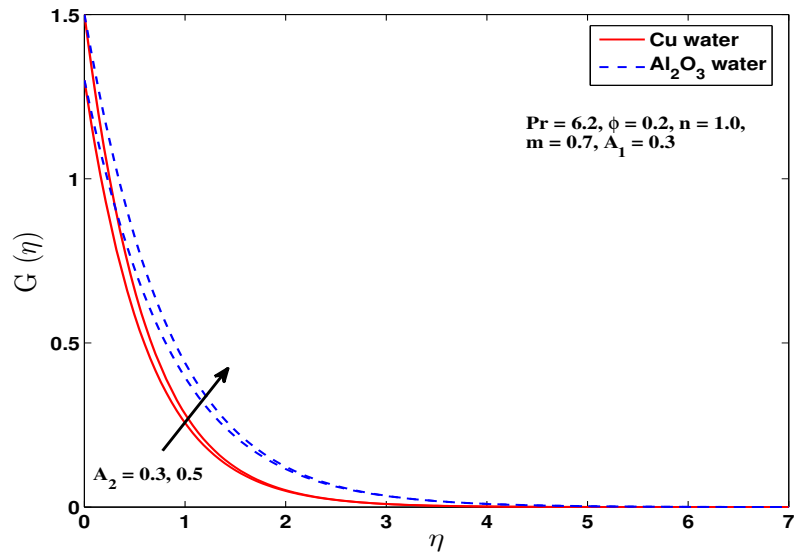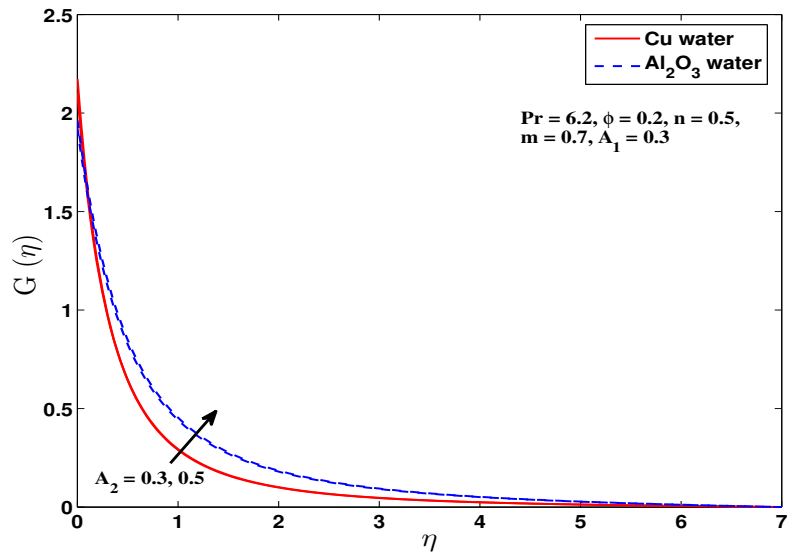Figure 5.34 – Present lines for tangential velocity for variation in A_2 when $n = 0.5$.
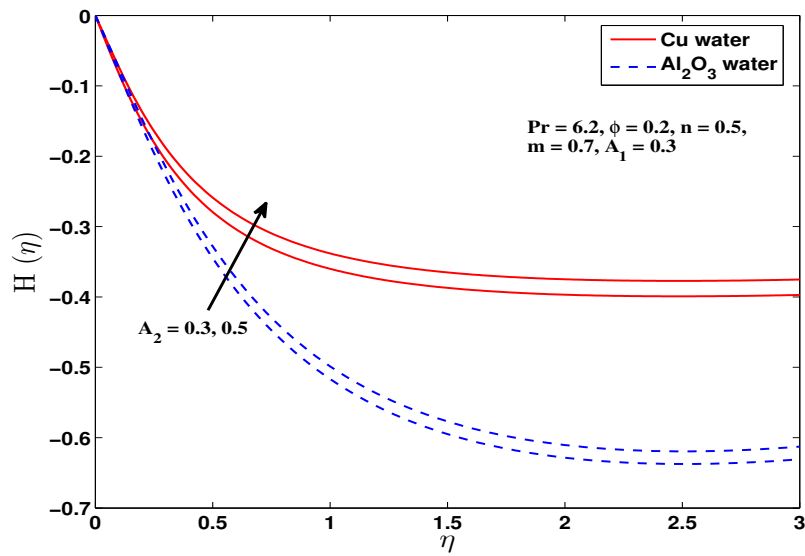
Figure 5.35 – Present lines for axial velocity for variation in A_2 when $n = 0.5$.

73
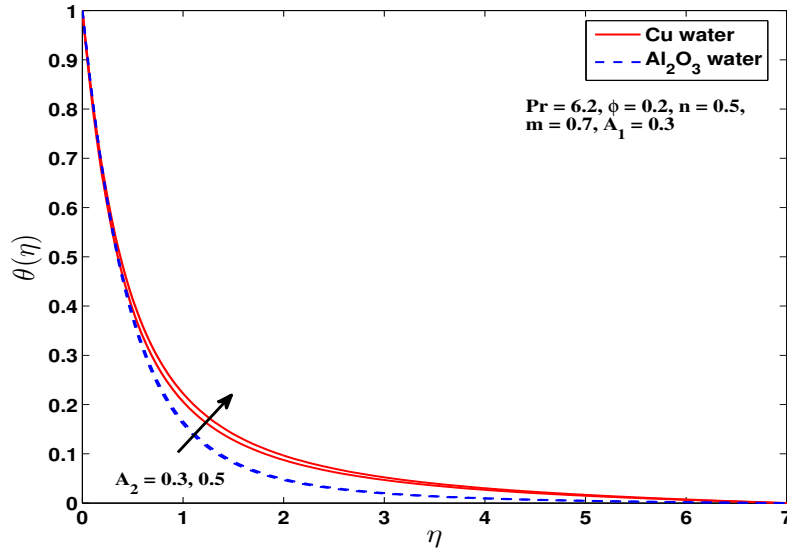
Figure 5.36 – Present lines for temperature profile for variation in A_2 when $n = 0.5$.

5.4.5 Skin friction coefficient:

The effect of POWER-LAW index n and nanoparticle volume fraction ϕ on skin friction coefficient remains the same as discussed in section 4.4.3 of the previous chapter. The Table 5.2 shows the impact of parameters m and velocity slip parameters A_1 and A_2 on skin friction coefficient at the disk. It is observed that at the disk values of skin friction coefficient rise with an increase in magnetic parameter m due to the production of Lorentz force. Also an increase in slip parameters A_1 and A_2 cause increase in skin friction coefficient.

Table 5.2 – Values of skin friction coefficient for the variation of parameters for fixed $Pr = 6.2$.

m	A_1	A_2	$C_f Re_r^{1/n+1}$ Cu - water	$C_f Re_r^{1/n+1}$ $Al_2O_3 - water$
0.3	0.3	0.5	3.5536	2.5288
0.5			3.7351	2.6196
0.7			3.9189	2.7125
	0.1		3.8418	2.6474
	0.3		3.9189	2.7125
		0.3	3.2612	2.2496
		0.5	3.9189	2.7125

5.4.6   Nusselt number:

The effect of POWER-LAW index n and nanoparticle volume fraction ϕ on Nusselt number remains the same as discussed in section 4.4.4 of the previous chapter. The Table 5.3 shows the impact of parameters m and velocity slip parameters A_1 and A_2 on Nusselt number at the disk. At the disk Nusselt number decrease with an increase in magnetic parameter m due to a decrease in heat transfer rate. Both the increase in the slip parameters A_1 and A_2 increases the heat transfer rate and thus the Nusselt number.

Table 5.3 – Values of Nusselt Number for the variation of parameters for fixed Pr = 6.2.

m	A_1	A_2	$-Nu_r Re_r^{-1/n+1}$ Cu - water	$-Nu_r Re_r^{-1/n+1}$ $Al_2O_3 - water$
0.3	0.3	0.5	-1.4767	-1.5917
0.5			-1.4223	-1.5568
0.7			-1.3671	-1.5211
	0.1		-1.0902	-1.2124
	0.3		-1.3671	-1.5211
		0.3	-1.3325	-1.4943
		0.5	-1.3671	-1.5211

Chapter 6

CONCLUSION AND RECOMMENDATIONS

In this thesis we studied the analysis of MHD slip flow with heat transfer of Cu-water and Al_2O_3-water based nanofluids with variable thermal conductivity obeying POWER-LAW model over an infinite rotating disk in detail. The velocity slip conditions are used. Also thermal conductivity is assumed to be the function of velocity gradients (same as viscosity function). The governing PDEs were first reduced to ODEs. The new system was then solved with the help of MATLAB *bvp4c* code and results are displayed in the form of tables and graphs.

We can draw the following results and conclusions from our research:

- The main use of nanoparticles is to boost the thermal behavior of the fluid. Therefore increase in nanoparticles concentration enhances both the temperature of nanofluid and thermal boundary layer thickness. Also increase in ϕ cause rise in skin friction coefficient by decreasing the nanofluid's velocity.

- As we enhance the POWER-LAW index n, the thickness of boundary layer decreases.

- As the strength of magnetic field increases, the nanofluid's velocity decreases and its temperatures rises.

- Increase in velocity slip parameter lowers the magnitude of velocity as well as thickness of velocity boundary layer while inside the boundary layer it increases the rate of heat transfer.

Current model has revealed significant results to focus on slip effects and variable thermal conductivity of the flow which include nanofluids over a rotating disk. Future investigations may involve the study using viscosity and thermal conductivity of non-Newtonian fluids which depends on temperature. An interesting area for further inspecting in the future would be the study of above mentioned effects on the third grade fluid. There is an option to conduct experimental studies on such systems.

Bibliography

[1] J. C. Maxwell, A Treatise on Electricity and Magnetism, *2nd ed., Clarendon Press: Oxford, UK*, (1881).

[2] S. U. S. Choi, Enhancing thermal conductivity of fluids with nanoparticles, *ASME International Mechanical Engineering Congress and Exposition, San Francisco, CA (United States)*, **66** (1995) 99-105.

[3] J. A. Eastman, S. U. S. Choi, S. Li, W. Yu, and L. J. Thompson, Anomalously increased effective thermal conductivities of ethylene glycol-bases nanofluids containing copper nanoparticles, *Appl. Phys. Lett.*, **78(6)** (2001).

[4] X. Wang, X. Xu, S. U. S. Choi, Thermal conductivity of nanoparticle-fluid mixture, *J. Thermophys. Heat. Tr.*, **13** (1999) 474–480.

[5] P. Keblinski, S. RPhillpot, S. U. S. Choi, J. A. Eastman , Mechanisms of heat flow in suspension of nano-sized particles (nanofluids), *Int. J. Heat Mass Trans.*, **45** (2002) 855–863.

[6] J. Buongiorno, Convective transport in nanouids, *ASME J. Heat Transfer*, **128** (2006) 240–250.

[7] P. Keblinski, J. A. Eastman, D. G. Cahill, Nanouids for thermal transport, *Mater. Today*, **8** (2005) 36–44.

[8] X. Q. Wang, A. S. Mujumdar, Heat transfer characteristics of nanouids: A review, *Int. J. Therm. Sci.*, **46** (2007) 1–19.

[9] A. Noghrehabadi , M. Ghalambaz , A. Ghanbarzadeh, Effects of variable viscosity and thermal conductivity on natural convection of nanofluids past a vertical plate in porous media, *J. Mechanics*, **30** (2014) 265–275.

[10] A. J. Jaffri, M. W. Bhat, G. Vyas, A. Kumar, R. S. Dondapati, A review on the recent development in enhancing the thermal conductivity in nanofluids, *International Journal of Mechanical Engineering and Technology*, **8(7)** (2017) 1540–1545.

[11] P. Keblinski, S. R. Phillpot, S. U. S. Choi, J. A. Eastman, Mechanisms of heat flow in suspensions of nano-sized particles (nanofluids), *Int. J. Heat Mass Trans.*, **45** (2002) 855–863.

[12] T. Yiamsawasd, A. S. Dalkilic, S. Wongwises, Measurement of specific heat of nanofluids, *Curr. Nanosci.*, **10** (2012) 25–33.

[13] M. Turkyilmazoglu, Nanofluid flow and heat transfer due to a rotating disk, *Comput. Fluids*, **94** (2014) 139-146.

[14] O. Makinde and A. Aziz, Boundary layer flow of a nanofluid past a stretching sheet with a convective boundary condition, *Int. J. Therm. Sci.*, **50**, (2011) 1326–1332.

[15] T. Hayat, S. Qayyum, M. Imtiaz, F. Alzahrani, A. Alsaedi, Partial slip effect in flow of magnetite Fe3O4 nanoparticles between rotating stretchable disks, *J. Magn. Magn. Mater.*, **413** (2016) 39–48.

[16] M. J. Uddin, I. Pop, A. I. M. Ismail, Free convection boundary layer flow of a nanofluid from a convectively heated vertical plate with linear momentum slip boundary condition, *Sains Malaysiana*, **41(11)** (2012) 1475–1482.

[17] W. Ibrahim, B. Shankar, MHD boundary layer flow and heat transfer of a nanofluid past a permeable stretching sheet with velocity, thermal and solutal slip boundary conditions, *Comput. Fluids*, **75** (2013) 1–10.

[18] R. Sharma, A. Ishak, Second order slip flow of Cu-water nanofluid over a stretching sheet with heat transfer, *WSEAS Transactions on Fluid Mechanics*, **9** (2014). 26–33.

[19] R. Ellahi, M. Hassan, A. Zeeshan, Shape effects of nanosized particles in Cu H2O nanofluid on entropy generation, *Int. J. Heat Mass Trans.*, **81** (2015) 449–456.

[20] E. Abu-Nada and A. J. Chamkha, Effect of nanofluid variable properties on natural convection in enclosures filled with a CuO-EG-Water nanofluid, *Int. J. Therm. Sci.*, **49** (2010) 2339–2352.

[21] K. V. Wong, O. D. Leon, Applications of nanofluids: current and future, *Adv. Mech. Eng.*, **2010** (2010) 1–11 .

[22] R. Saidur, S. N. Kazi, M. S. Hossain, M. M. Rahman, H. A. Mohamed, A review on the performance of nanoparticles suspended with refrigerants and lubricating oils in refrigeration systems, *Renew. Sust. Energ. Rev.*, **15(1)** (2011) 310–323.

[23] W. G. Cochran, The flow due to a rotating disk, *Math. Proc. Cambridge*, **30** (1934) 365–375.

[24] K. Stewartson, On the flow between two rotating coaxial disks, *Math. Proc. Cambridge*, **49** (1953) 333–341.

[25] C. Y. Ming, L. C. Zheng, X. X. Zhang, Steady flow and heat transfer of the power-law fluid over a rotating disk, *Int. Commun. Heat Mass*, **38** (2011) 280–284.

[26] I. Pop, M. Rashidi, R.S.R. Gorla, Mixed convection to power-law type non-Newtonian fluids from a vertical wall, *Polym. Plast. Technol.*, **30** (1991) 47–66.

[27] I. Pop, Boundary layer flow at a three-dimensional stagnation point in power-law non-Newtonian fluids, *Int. J. Heat Fluid Fl.*, **14** (1993) 408–412

[28] M. Kumari, T. Grosan, I. Pop, Rotating flows of power-law fluids over a stretching surface, *Technische Mechanik*, **1** (2006) 11–19.

[29] J. A. Khan, M. Mustafa, A. Mushtaq, On three-dimensional flow of nanofluids past a convectively heated deformable surface: A numerical study, *Int. J. Heat Mass Tran.*, **94** (2016) 49–55.

[30] C. Y. Ming, L. C. Zheng, X. X. Zhang, F. Liu, V. Anh, Flow and heat transfer of the power-law fluid over a rotating disk with generalized diffusion, *Int. Commun. Heat Mass*, **79** (2016) 81–88.

[31] A. A Saleem, R. Fathy, MHD flow and heat transfer of non-Newtonian power-law nanofluid over a rotating disk with Hall current, *Therm. sci.*, **22** (2018) 171–182.

[32] T. V. Karman, Uber laminare und turbulente Reibung, *Z. Angew. Math. Mech.*, **1(4)** (1921) 233–252.

[33] P. Mitschka, Nicht-Newtonsche Flüssigkeiten II. Drehströmungen Ostwald-de Waelescher Nicht-Newtonsche Flüssigkeiten, *Collect. Czech. Chem. Commun.*, **29** (1964) 2892–2905.

[34] P. Mitschka, J. Ulbrecht, Nicht-Newtonsche Flüssigkeiten IV. Strömung Nicht-newtonsche Flüssigkeiten Ostwald-de Waelescher Typs in der Umgebung Rotierender Drehkegel und Schieben, *Collect. Czech. Chem. Commun.*, **30** (1965) 2511–2526.

[35] H.I. Andersson, E. de Korte, R. Meland, Flow of a power-law fluid over a rotating disk revisited, *Fluid Dyn. Res.*, **28** (2001) 75–88.

[36] A. K. Santra, S. Sen, N. Chakraborty, The forced convection of Cu-water nanofluid in a channel with both Newtonian and Non-Newtonian models, *Int. J. Therm. Sci.*, **48** (2009) 391–400.

[37] L. C. Zheng, X. X. Zhang, J. C. He, Suitable heat transfer model for self-similar laminar boundary layer in power law fluids, *J. Therm. Sci.*, **13** (2004) 150–154.

[38] L. C. Zheng, X. X. Zhang, C. Q. Lu, Heat transfer of power law non-Newtonian fluids, *Chinese Phys. Lett.*, **23** (2006) 3301–3304.

[39] L. C. Zheng, X. X. Zhang, J. C. He, Existence and estimate of positive solutions to a nonlinear singular boundary value problem in the theory of dilatant non-Newtonian fluids, *Math. Comput. Model*, **45** (2007) 387–393.

[40] L. C. Zheng, X. X. Zhang, L. X. Ma, Fully developed convective heat transfer for power law fluids in a circular tube, *Chinese Phys. Lett.*, **25** (2008) 195–197.

[41] B. Li, L. Zheng, X. Zhang, Heat transfer in pseudo-plastic non-Newtonian fluids with variable thermal conductivity, *Energ. Convers. Manage.*, **52** (2011) 355–358.

[42] L. C. Zheng, Y. H. Lin, X. X. Zhang, Marangoni convection of power law fluids driven by power-law temperature gradient, *J. Franklin Inst.*, **349** (2012) 2585–2597.

[43] H. I. Andersson, E. de Korte, MHD flow of a power-law fluid over a rotating disk , *Eur. J. Mech. B-Fluid*, **21** (2002) 317–324.

[44] S. Y. Lee, W. F. Ames, Similar solutions for non-newtonian fluids, *AICHE J.*, **12** (1966) 700–708.

[45] H. I. Andersson, K. H. Bech, B. S. Dandapat, Magnetohydrodynamic flow of a power law fluid over a stretching sheet, *Int. J. Nonlinear Mech.*, **72** (1992) 929–936.

[46] M. A. A. Mahmoud, M. A. E. Mahmoud, Analytical solutions of hydromagnetic boundary layer flow of a non-Newtonian power-law fluid past a continuously moving surface, *Acta Mech.*, **181** (2006) 83–89.

[47] C. Y. Cheng, Combined heat and mass transfer in natural convection flow from a vertical wavy surface in a power-law fluid saturated porous medium with thermal and mass stratification, *Int. Commum. Heat and Mass*, **36** (2009) 351–356.

[48] D. Pal, S. Chatterjee, Soret and dufour effects on MHD convective heat and mass transfer of a power-law fluid over an inclined plate with variable thermal conductivity in a porous medium, *Appl. Math. Comput.*, **219** (2013) 7556–7574.

[49] R. Shyam, C. Sasmal, R. P. Chhabra, Natural convection heat transfer from two vertically aligned circular cylinders in power-law fluids, *Int. J. Heat Mass Tran.*, **64** (2013) 1127–1152.

[50] M. H. Yazdi, I. Hashim, L. K. Moey, K. Sopian, Slip velocity effect on non-Newtonian fluid flow over moving permeable surface with nonlinear velocity and internal heat generation/absorption, *International Review on Modelling and Simulations*, **7(4)** (2014) 661–670.

[51] T. Hayat, M. Hussain, A. Alsaedi, S. A. Shehzad, G. Q. Chen, Flow of power law nanofluid over a stretching surface with Newtonian heating, *J. Appl. Fluid Mech.*, **8** (2015) 273–280.

[52] M. Ramzan, J. D. Chung, M. Bilal, U. Farooq, Mixed convective flow of Maxwell nanofluid past a porous vertical stretched surface – An optimal solution, *Results Phys.*, **6** (2016) 1072–1079.

[53] T. Hayat, T. Hussain, S. A. Shezad, A. Alsaedi, Flow of Oldroyd-B fluid with nanoparticles and thermal radiation, *Appl. Math. Mech.–Engl.*, **36(1)** (2015) 69–80.

[54] T. Hayat, S. Qayyum, M. Imtiaz, A. Alsaedi, MHD flow and heat transfer between coaxial rotating stretchable disks in a thermally stratified medium, *PLOS One*, **11** (2016) .

[55] T. Hayat, M. Tamoor, M. Imtiaz, A. Alsaedi, Numerical simulation for nonlinear radiative flow by convective cylinder, *Results Phys.*, **6** (2016) 1031–1035.

[56] T. Hayat, S. Qayyum, M. Imtiaz, A. Alsaedi, Flow between two stretchable rotating disks with CattaneoChristov heat flux model, *Results Phys.*, **7** (2017) 126–133.

[57] T. Hayat, S. Qayyum, M. Imtiaz, A. Alsaedi, Radiative Falkner–Skan flow of Walter-B fluid with prescribed surface heat flux, *J. Theor. Appl. Mech.*, **55(1)** (2017) 117–127.

[58] H. C. Brinkman, The viscosity of concentrated suspensions and solutions, *J. Chem. Phys.*, **20(4)** (1952) 571.

[59] K. Khanafer, K. Vafai and M. Lightstone, Buoyancy-driven heat transfer enhancement in a two-dimensional enclosure utilizing nanofluids. *Int. J. Heat Mass Tran.*, **46** (2003) 3639–3653.

[60] T. Cebeci, P. Bradshaw, Physical and Computational Aspects of Convective Heat Transfer, *Springer-Verlag, New York*, **Chap: 13** (1988).